

UNIVERSITÉ DU QUÉBEC À MONTRÉAL

ANALYSE DE PERFORMANCE D'UN MODÈLE RÉGIONAL  
DU CLIMAT À SIMULER LA VARIABILITÉ DE LA  
PRÉCIPITATION ASSOCIÉE AU FORÇAGE ENSO DANS  
LES TROPIQUES AMÉRICAINES

MÉMOIRE

PRÉSENTÉ

COMME EXIGENCE PARTIELLE

DE LA MAÎTRISE EN SCIENCES DE L'ATMOSPHÈRE

PAR

ETIENNE TOURIGNY

OCTOBRE 2008

UNIVERSITÉ DU QUÉBEC À MONTRÉAL  
Service des bibliothèques

Avertissement

La diffusion de ce mémoire se fait dans le respect des droits de son auteur, qui a signé le formulaire *Autorisation de reproduire et de diffuser un travail de recherche de cycles supérieurs* (SDU-522 – Rév.01-2006). Cette autorisation stipule que «conformément à l'article 11 du Règlement no 8 des études de cycles supérieurs, [l'auteur] concède à l'Université du Québec à Montréal une licence non exclusive d'utilisation et de publication de la totalité ou d'une partie importante de [son] travail de recherche pour des fins pédagogiques et non commerciales. Plus précisément, [l'auteur] autorise l'Université du Québec à Montréal à reproduire, diffuser, prêter, distribuer ou vendre des copies de [son] travail de recherche à des fins non commerciales sur quelque support que ce soit, y compris l'Internet. Cette licence et cette autorisation n'entraînent pas une renonciation de [la] part [de l'auteur] à [ses] droits moraux ni à [ses] droits de propriété intellectuelle. Sauf entente contraire, [l'auteur] conserve la liberté de diffuser et de commercialiser ou non ce travail dont [il] possède un exemplaire.»

## REMERCIEMENTS

Je tiens à remercier mon directeur de recherche, Dr. Colin G. Jones, pour sa patience, sa rigueur scientifique et son dévouement pour la recherche. Je remercie également Sara A. Rauscher du Earth System Physics à l'Abdus Salam International Centre for Theoretical Physics (ICTP) pour son aide et inspiration, Dave Allured et Brant Liebmann du Climate Analysis Branch de la National Oceanic and Atmospheric Administration (NOAA) pour la grille d'observation journalière en Amérique du Nord, ainsi que Anders Ullerstig et Patrick Samuelsson du Rossby Center au Swedish Meteorological and Hydrological Institute (SMHI) pour la préparation des conditions frontières utilisées par le modèle régional du climat RCA. Cette étude a été rendue possible grâce au soutien financier du Réseau canadien en modélisation et diagnostics du climat régional (MDCR) et ses partenaires ainsi qu'au matériel informatique fourni par le consortium Ouranos et le Rossby Center du SMHI en Suède.

## TABLE DES MATIÈRES

LISTE DES FIGURES . . . . .	vii
LISTE DES TABLEAUX . . . . .	xi
LISTE DES ABRÉVIATIONS, SIGLES ET ACRONYMES . . . . .	xiii
RÉSUMÉ . . . . .	xv
ABSTRACT . . . . .	xvii
INTRODUCTION . . . . .	1
CHAPITRE I	
ARTICLE I : ÉCHELLE SAISONNIÈRE . . . . .	7
ABSTRACT . . . . .	9
1.1 Introduction . . . . .	11
1.2 Model and data . . . . .	14
1.2.1 Domain of study and regions . . . . .	14
1.2.2 Model setup . . . . .	14
1.2.3 Observations . . . . .	16
1.3 Climatology . . . . .	18
1.3.1 Methodology . . . . .	18
1.3.2 Results . . . . .	18
1.4 Interannual variability . . . . .	23
1.4.1 A review of ENSO effects and teleconnections . . . . .	23
1.4.2 Methodology . . . . .	25
1.4.3 Results . . . . .	26
1.5 Assessing the benefits of increased resolution . . . . .	32
1.6 Conclusions . . . . .	34
CHAPITRE II	
ARTICLE II : ÉCHELLE INTRASAISONNIÈRE . . . . .	49
ABSTRACT . . . . .	51

2.1	Introduction . . . . .	53
2.2	Model Configuration and Analysis Methods . . . . .	56
2.2.1	Observations . . . . .	56
2.2.2	Methods . . . . .	57
2.3	Results . . . . .	59
2.3.1	Annual Cycle of Precipitation . . . . .	59
2.3.2	Rainy Season Onset, Demise and Duration . . . . .	61
2.3.3	Intensity distribution of precipitation . . . . .	65
2.4	Discussion and Conclusions . . . . .	71
	CONCLUSION . . . . .	83
	RÉFÉRENCES . . . . .	85

## LISTE DES FIGURES

1.1	Domain of the study and chosen regions. The dashed box shows the area of analysis. . . . .	35
1.2	Climatological SLP (contours in hPa) and 925 hPa winds (vectors in m/s) in left column, 250 hPa geopotential height (contours in dam) and winds (vectors in m/s) in right column. The scale of the wind vectors is indicated on each figure. . . . .	36
1.3	Climatological precipitation (mm/day) / seasons JFM and JAS (columns) / GPCP, CRU, ECMWF and RCA (rows). . . . .	37
1.4	Spatial mean climatological precipitation over land, annual cycle by region. The duration of the climatological rainy season is indicated for each region on the x-axis. . . . .	38
1.5	Climatological average of July and August minus the average of June and September precipitation (mm/day). . . . .	39
1.6	El Niño anomalies ( <i>NINOA</i> ) of : SLP (contours in hPa) and 925 hPa winds (vectors in m/s) in left column, 250 hPa geopotential height (contours in dam) and winds (vectors in m/s) in right column. Full lines indicate positive anomalies and dotted lines indicate negative anomalies. The scale of the wind vectors is indicated on each figure. . . . .	40
1.7	El Niño anomalies ( <i>NINOA</i> ) of precipitation (mm/day) / seasons JAS(0) and JFM(+) (columns) / GPCP, CRU, ECMWF and RCA (rows). . . .	41
1.8	As Figure 1.7 but La Niña anomalies ( <i>NINAA</i> ) of precipitation (mm/day). . . .	42

1.9	El Niño (left column) and La Niña (right column) anomalies of precipitation (mm/day) over land, annual cycle by region. The typical period and impact (wet/dry) of ENSO variability for each region is indicated on the x-axis. The scales on the y-axis are different in each plot. . . . .	43
1.10	Time series of precipitation anomalies over land (mm/day) / regions (a) CAR(season JAS) (b) NAMZ(season JFM) and (c) MEX(season JFM); (d) Niño 3.4 SST anomaly (°C). . . . .	44
1.11	Climatological precipitation (mm/day) during the 1998-2005 period / seasons JFM and JAS (columns) / GPCP, TRMM, RCA and RCA1 (rows). . . . .	45
1.12	Precipitation anomaly (mm/day) during the 1999-2000 La Niña / seasons JAS(0) and JFM(+) (columns) / GPCP, TRMM, RCA and RCA1 (rows). . . . .	46
2.1	Spatial mean climatological precipitation (top rows) and El Niño anomalies of precipitation (bottom row), annual cycle by region over land (mm/day). The duration of the climatological rainy season and the typical period and impact (wet/dry) of ENSO variability are indicated for each region on the x-axis. . . . .	74
2.2	Onset and demise dates of the rainy season over land by region. Where a mark is not visible it is coincident with another mark. El Niño years are shown in large grey tick marks and La Niña years in large black tick marks on the x-axis. . . . .	75

- 2.3 Precipitation intensity distribution (% of pentads) over land during yearly computed rainy seasons / climatological frequency of occurrence (top row), climatological accumulated precipitation for each intensity bin (second row) and anomalies in binned frequency of occurrence for El Niño and La Niña years (bottom rows) / regions CAR, CAM, NAMZ and MEX (columns). The scales on the y-axis are different in each plot. . . . 76
- 2.4 As Figure 2.3 but for NAMZ region using a fixed rainy season February-July (left column), MEX region using a fixed dry season January-March (right column). . . . . 77
- 2.5 Precipitation intensity distribution (% of pentads) over land during yearly computed rainy seasons during the 1998-2004 period / climatological frequency of occurrence (top row), climatological accumulated precipitation for each intensity bin (bottom row) / regions CAR and NAMZ (left and right columns). The scales on the y-axis are different in each plot. . . . 78
- 2.6 Frequency of occurrence of pentad-mean precipitation in excess of 10 mm/day (in % of total precipitation intensity occurrence) for June-September / GPCP, ECMWF and RCA (columns) / Climatology (top row), El Niño anomalies (*NINOA*) during JAS(0) season (middle row) and La Niña anomalies (*NINAA*) during JAS(0) season (bottom row). . . . . 79
- 2.7 Frequency of occurrence of pentad-mean precipitation in excess of 10 mm/day (in % of total precipitation intensity occurrence) for June-September during the 1998-2004 period. . . . . 80

## LISTE DES TABLEAUX

1.1	Strong ENSO events in the 1979-2005 period . . . . .	47
1.2	Linear correlation (RCA vs. observations and ECMWF vs. observations) of seasonal anomalies of precipitation over land. Bold values are significant at 99% level, others at 95% level (except those in parentheses). . .	47
2.1	Climatological Onset and Demise (month-day) and Length (in days) of Rainy Season by Region and changes (in days) in the Onset, Demise and Length for El Niño and La Niña years. . . . .	81

## LISTE DES ABRÉVIATIONS, SIGLES ET ACRONYMES

AGCM	Atmosphere only General Circulation Model
CAM	Amérique Centrale (région étudiée)
CAR	Caraïbes (région étudiée)
CGCM	Coupled Ocean-Atmosphere General Circulation Model
CRU	Climatic Research Unit TS 2.1 (observation utilisée)
ECMWF	European Centre for Medium-Range Weather Forecasts
ERA40	ECMWF Reanalysis
ENSO	El Niño/Southern Oscillation
GCM	General Circulation Model
GPCP	Global Precipitation Climatology Project (observation utilisée)
ICTP	Abdus Salam International Centre for Theoretical Physics
ITCZ	Inter Tropical Convergence Zone
JRA25	Japanese Reanalysis
LANA	Liebmann-Allured NA1 (observation utilisée)
LASA	Liebmann-Allured South America (observation utilisée)
LBC	Lateral Boundary Conditions
MCG	Modèle de Circulation Générale
MSD	Mid-Summer Drought
MEX	Nord du Mexique (région étudiée)
MRC	Modèle Régional du Climat
NAMZ	Nord de l'Amazonie (région étudiée)
NINOA	Anomaly of the El Niño composite
NINAA	Anomaly of the La Niña composite
NOAA	National Oceanic and Atmospheric Administration

ONI	Oceanic Niño Index
PNA	Pacific/North American
RCA	Rosby Center Atmospheric Model version 3, résolution de 0.33°
RCA1	Rosby Center Atmospheric Model version 3, résolution de 1°
RCM	Regional Climate Model
SLP	Sea Level Pressure
SMHI	Swedish Meteorological and Hydrological Institute
SST	<i>Sea Surface Temperature</i> , température de la surface de la mer
SSTA	Sea Surface Temperature Anomaly
TKE	Turbulent Kinetic Energy
TJ2008a	Premier article de l'étude, échelle saisonnière
TJ2008b	Second article de l'étude, échelle intrasaisonnière
TRMM	Tropical Rainfall Measuring Mission (observation utilisée)

## RÉSUMÉ

La prévision d'anomalies saisonnières et intrasaisonnières des précipitations est utile dans des domaines tels que l'agriculture et la gestion de l'eau, ainsi que dans la prévention des catastrophes climatiques dans les pays tropicaux. Les anomalies de température de la surface de la mer (*Sea Surface Temperature* ; SST) associées au forçage El Niño/Southern Oscillation (ENSO) constituent une source majeure de prévisibilité dans les tropiques. En effectuant une mise à l'échelle dynamique des prévisions de modèles de circulation générale (MCG), les modèles régionaux du climat (MRC), grâce à leur résolution accrue, pourraient permettre une bonne prévision de ces anomalies saisonnières et intrasaisonnières dans les tropiques.

Cette étude constitue une évaluation de l'habilité d'un MRC (le Rossby Center Regional Atmospheric Model version 3 ; RCA) à effectuer une mise à l'échelle des anomalies de SST et circulation de grande échelle associées au forçage ENSO. RCA est configuré sur un domaine comprenant l'est de l'Océan Pacifique tropical et les tropiques américaines, et il est exécuté pour 27 années différentes pour la période 1979-2005. Le modèle utilise comme conditions aux frontières les SST observées et les réanalyses du European Centre for Medium-Range Weather Forecasts (ECMWF) pour la circulation de grande échelle. Nous étudions la performance de RCA à représenter les patrons régionaux de précipitation dans les tropiques américaines, en se concentrant sur la climatologie et la variabilité saisonnière et intrasaisonnière associée à ENSO. Les statistiques intrasaisonnières à l'étude sont la distribution de l'intensité de précipitation ainsi que les moments de transition entre les saisons sèches et humides.

Deux articles acceptés pour publication dans la revue *Tellus Series A : Dynamic Meteorology and Oceanography* sont présentés ici, le premier se concentrant sur l'échelle saisonnière et le second sur l'échelle intrasaisonnière. Il est démontré que le modèle RCA reproduit la majorité des caractéristiques régionales de la précipitation ainsi que la variabilité de la précipitation associée à ENSO. Cette étude est une évaluation préliminaire pour le modèle RCA, qui devrait être suivie par une analyse plus poussée qui utiliserait des conditions aux frontières provenant d'un MCG.

Mots clés : Modèle Régional du Climat, ENSO, variabilité interannuelle, précipitation, tropiques américaines

## ABSTRACT

Forecasting of seasonal and subseasonal anomalies of precipitation is useful in fields such as agriculture and water resource management, as well as in climate disaster prevention in tropical countries. Anomalies in sea surface temperature (SST) associated to El Niño/Southern Oscillation (ENSO) forcing constitute a major source of predictability in the tropics. Predictions of General Circulation Models (GCMs) can be dynamically downscaled by Regional Climate Models (RCMs). The increased spatial resolution of RCMs can potentially make good predictions of these seasonal and subseasonal anomalies in the tropics.

This study represents an evaluation of the ability of a RCM (the Rossby Center Regional Atmospheric Model version 3; RCA) to downscale SST and general circulation anomalies associated with ENSO forcing. RCA is configured over a domain comprising the tropical east Pacific Ocean and the tropical Americas, and is run for 27 different years for the period 1979-2005. The model boundary conditions are given by observed SSTs and re-analyses from the European Centre for Medium-Range Weather Forecasts (ECMWF). The performance of RCA to represent regional patterns of precipitation in the tropical Americas is studied, concentrating on the mean climatology and seasonal and subseasonal variability associated with ENSO. Evaluated subseasonal statistics encompass the intensity distribution of precipitation and the timing (onset and demise) of the rainy season.

Two articles accepted for publication in *Tellus Series A : Dynamic Meteorology and Oceanography* are presented here, the first concentrating on seasonal timescales and the second on subseasonal timescales. It is shown that the RCA model reproduces the major regional characteristics of precipitation as well as the variability of precipitation associated with ENSO. This study is a preliminary evaluation of the RCA model, which will be followed by a study using RCA with boundary conditions provided by a GCM.

Key words : Regional Climate Model, ENSO, interannual variability, precipitation, tropical americas

## INTRODUCTION

Les Modèles de Circulation Générale (MCG) sont utilisés depuis plusieurs années pour effectuer des projections climatiques à une échelle temporelle allant de l'échelle saisonnière (prévision saisonnière) à multi-décennale (projection de changements climatiques). La faible résolution spatiale des MCG, due aux contraintes en matière de calcul numérique, nécessite le paramétrage de nombreux phénomènes de sous-échelles et ne résout pas bien les phénomènes orographiques. Les Modèles Régionaux du Climat (MRC), de par leur haute résolution spatiale, sont employés pour pallier à ces problèmes et fournir une projection plus détaillée et potentiellement plus réaliste au-dessus d'une région donnée.

Dans les régions tropicales, les variations de la température de la surface de la mer (*Sea Surface Temperature*; SST) sont la cause d'anomalies atmosphériques importantes à l'échelle saisonnière. Le phénomène couplé océan-atmosphère El Niño/Southern Oscillation (ENSO) réfère aux anomalies de SST dans l'Océan Pacifique tropical et aux perturbations concomitantes de la circulation atmosphérique, particulièrement dans les tropiques mais aussi en des endroits plus éloignés du globe. Les MCG couplés océan-atmosphère permettent une bonne prévision des anomalies de SST dans le Pacifique tropical à l'échelle saisonnière, et les MCG atmosphériques reproduisent relativement bien les anomalies de la circulation de grande échelle dans les tropiques. Par contre, les prévisions d'anomalies de précipitations faites par les MCG ne sont pas suffisamment détaillées pour être utilisées par les décideurs locaux dans des domaines tels que l'agriculture et la gestion de l'eau (Goddard et al., 2001). Depuis quelques années, les MRC sont utilisés avec succès dans des régions vulnérables des tropiques, telles que le Nord-Est du Brésil (Sun et al., 2006), en effectuant une mise à l'échelle dynamique des prévisions des MCG à l'échelle spatiale adéquate pour les usagers. La prévision sai-

sonnière à l'échelle régionale dans les régions tropicales représente un intérêt double, par son (relativement) grand potentiel prédictif émanant des anomalies de SST et la vulnérabilité des populations locales.

D'autre part, la prévision de la variabilité de la précipitation à petite échelle temporelle (distribution journalière de la précipitation et durée de la saison des pluies) est importante pour les décideurs locaux, notamment pour la planification agricole (Rauscher et al., 2007, et références incluses). La faible résolution spatiale des MCG rend difficile la prévision d'anomalies régionales à cette échelle temporelle. Les erreurs dues aux paramétrages de phénomènes de sous-échelle (tels que la convection) et à la résolution grossière de l'orographie causent des erreurs dans la distribution journalière de la précipitation. Les MRC, par leur représentation topographique accrue, offrent une meilleure représentation du climat à la fréquence journalière (Seth et al., 2004).

Le phénomène ENSO se mesure en anomalies de SST dans l'Océan Pacifique tropical et du gradient zonal de pression à la surface de la mer (*Sea Level Pressure* ; SLP) au-dessus de l'Océan Pacifique et se comporte de façon quasi-cyclique. La phase chaude d'ENSO (El Niño) se traduit par des températures des eaux de surface au centre et à l'est de l'Océan Pacifique tropical plus élevées que la normale et à une réduction du gradient climatologique est-ouest de SST (Philander, 1990). La phase froide (La Niña) se manifeste par une diminution de SST dans cette même zone. Dans un événement El Niño, il s'en suit une augmentation de la convection dans cette zone ce qui, par des télé-connections, cause des perturbations en terme de température et précipitations en d'autres régions du globe (Alexander et al., 2002). Afin de décrire la séquence des télé-connections, il est nécessaire d'introduire le concept de composite des événements ENSO (Ropelewski et Halpert, 1987, 1996). Sachant qu'un événement ENSO (El Niño ou La Niña) dure en moyenne deux ans, les années (0) et (+) représentent les deux années d'un événement ENSO « typique » (en effectuant la moyenne des événements El Niño ou La Niña). Le maximum d'anomalie (positive ou négative) de SST se trouve dans la saison OND(0), soit dans les mois d'octobre à décembre de l'année (0). Les

composites El Niño et La Niña sont traités séparément et dans une large mesure les anomalies du composite La Niña sont de signe contraire à celles du composite El Niño (Aceituno, 1988; Ropelewski et Halpert, 1989).

Lors d'un événement El Niño, l'augmentation de la convection dans le centre et l'est de l'Océan Pacifique tropical a pour conséquence une diminution locale de SLP et une modification des cellules atmosphériques de grande échelle dites de Walker (circulation zonale) et Hadley (circulation méridienne). Les conséquences à court terme de ce phénomène (au niveau des tropiques américaines) sont une augmentation de la subsidence et une diminution de la précipitation dans les Caraïbes dues au déplacement de la cellule de Walker et à l'intensification de la cellule de Hadley (Chiang et al., 2000). La diminution de SLP à l'est du Pacifique et son augmentation dans le bassin Atlantique tropical nord (qui augmente l'intensité des vents du nord-est, les alizés) impliquent, dans les basses couches, une convergence dans le Pacifique est tropical et une divergence dans le bassin des Caraïbes. Cette divergence est responsable d'une diminution de la convergence d'humidité, donc de précipitation, en Amérique Centrale et dans les Caraïbes (Giannini et al., 2000, 2001b). Enfield et Alfaro (1999) ont démontré que la sécheresse due à un événement El Niño devance la fin de la saison des pluies en Amérique Centrale (et la retarde dans le cas d'un événement La Niña). La modification de la cellule de Walker est aussi tenue pour responsable d'une augmentation de la subsidence et une diminution de la précipitation dans la région amazonienne et dans le nord-est du Brésil (Kousky et al., 1984).

Une série d'événements connue sous le nom de « Atmospheric Bridge » (« pont atmosphérique » ; Alexander et al., 2002) explique les réponses atmosphériques différées dans notre région d'étude. Le réchauffement troposphérique anormal au-dessus de l'Océan Pacifique crée une perturbation dans le patron *Pacific/North American* (PNA), un mode de variabilité interannuelle au-dessus de l'Océan Pacifique Nord et du sous-continent nord-américain (Horel et Wallace, 1981; Barnston et Livezey, 1987). Cette perturbation diminue le SLP et augmente la précipitation autour du Golfe du Mexique dans la saison

hivernale de l'année (+) (Giannini et al., 2001b). Au même moment, l'anomalie du PNA est responsable d'une diminution de SLP dans la région de l'anticyclone des Açores (*Atlantic subtropical High*) et, par conséquent, d'une diminution de l'intensité des alizés dans l'Atlantique tropical nord (Nobre et Shukla, 1996). Il s'en suit une réduction de la convergence d'humidité dans la région amazonienne au printemps (+), ce qui diminue la convection (Marengo, 1992; Marengo et Hastenrath, 1993) et cause un délai dans l'initiation (et dans une moindre mesure, un devancement de la fin) de la saison des pluies dans le nord de l'Amazonie (Liebmann et Marengo, 2001; Marengo et al., 2001). Finalement deux études (Seth et al., 2004; Rauscher et al., 2007) ont démontré que les épisodes de sécheresse dans le nord-est du Brésil et en Amazonie sont attribuables à une réduction dans la fréquence des journées de précipitation d'intensité modérée à forte et une diminution dans la fréquences de journées d'intensité de précipitation faible ou nulle. Ces changements dans la distribution journalière de précipitation ont été relativement bien simulés par RegCM3, le MRC employé dans ces deux études.

Le présent ouvrage rend compte d'une étude qui a été faite sur un MRC, le Rossby Center Atmospheric Model version 3 (RCA) du Rossby Center en Suède, afin d'évaluer sa performance à simuler la variabilité de précipitation à l'échelle régionale dans les tropiques américaines due aux perturbations liées au phénomène ENSO, pour la période 1979-2005. Deux articles, rédigés en anglais avec le soutien et la collaboration de mon directeur de recherches Colin Jones, ont été soumis à la revue *Tellus Series A : Dynamic Meteorology and Oceanography* (acceptés avec révision). Le premier article (Tourigny et Jones, 2008a) se concentre sur la variabilité de la précipitation à l'échelle saisonnière, alors que le second (Tourigny et Jones, 2008b) traite de la variabilité à l'échelle intrasaisonnière, précisément à une fréquence de cinq jours (pentad). Ces deux articles composent les deux chapitres du présent ouvrage. Le domaine d'étude comprend l'Océan Pacifique tropical est, le Mexique, l'Amérique Centrale, les Caraïbes et le nord de l'Amérique du Sud (voir la Figure 1.1). L'analyse repose essentiellement sur une évaluation de la performance du modèle au niveau climatologique, ainsi qu'au niveau des composites ENSO, qui sont représentés par des moyennes des années El Niño et La

Niña (séparément) durant la période d'analyse. Ceci est fait en comparant les résultats du modèle aux réanalyses ERA-40 du European Centre for Medium-Range Weather Forecasts (ECMWF) ainsi qu'à plusieurs sources de données observées à l'échelle mensuelle et pentad, décrites dans les sections 1.2.3 et 2.2.1. L'absence de source d'observations à la fréquence journalière, sur l'ensemble du domaine et de la période d'analyse, nous a limité à utiliser des observations à la fréquence de pentad.

Le modèle RCA a été configuré avec une résolution spatiale de  $0.33^\circ$  en utilisant les données ERA-40 de ECMWF comme conditions aux frontières latérales et de surface. Les perturbations dues à ENSO sont incluses dans les champs de SST et dans les champs atmosphériques provenant des conditions aux frontières. Pour chaque année de la période 1979-2005, le modèle a été exécuté pour une période de 13 mois en utilisant les conditions initiales de ERA-40 de décembre de l'année précédente, ceci afin de se rapprocher du caractère « prévision saisonnière » de l'étude, par opposition à une étude sur les changements climatiques où les intégrations se font de façon continue. Les contraintes de calcul nous ont malheureusement empêché d'utiliser la technique d'ensemble qui s'applique à une prévision saisonnière en bonne et due forme. Cette technique consiste à effectuer plusieurs simulations avec des conditions initiales légèrement différentes et contribue à identifier la variabilité naturelle du système et à effectuer une prévision plus fiable et dont les incertitudes sont mieux identifiées. Plus de détails sur le modèle RCA et sa configuration pour cette étude sont donnés dans le premier article ci-inclus (voir la section 1.2.2). Notre étude est vue comme une évaluation préliminaire du modèle RCA à simuler les anomalies régionales de la précipitation associées au forçage ENSO. Cette étude en est également une de transférabilité, puisque le modèle Suédois RCA a été développé et testé dans une région différente, au climat sub-arctique et non tropical. Une étude plus détaillée verrait le même modèle forcé par des conditions latérales provenant d'un MCG.

## CHAPITRE I

### ARTICLE I : ÉCHELLE SAISONNIÈRE

**An Analysis of Regional Climate Model Performance Over the Tropical  
Americas. Part I : Simulating Seasonal Variability of Precipitation  
Associated with ENSO Forcing**

Etienne Tourigny

Université du Québec à Montréal, Montréal, Canada

Colin G. Jones

Université du Québec à Montréal, Montréal, Canada

Submitted to Tellus (April 3, 2008)

First revision (October 2, 2008)

## ABSTRACT

Sea surface temperature (SST) anomalies associated with El Niño/Southern Oscillation (ENSO) constitute a major source of predictability in the tropics. We evaluate the ability of a Regional Climate Model (the Rossby Center Atmospheric Model; RCA) to downscale SST and large scale atmospheric anomalies associated with ENSO. RCA is configured over the tropical East Pacific and tropical Americas and run for the period 1979-2005, using ECMWF lateral and surface boundary conditions. We study the ability of RCA to represent regional patterns of precipitation, with respect to both the climatology and interannual variability associated with ENSO. The latter is achieved by grouping the simulations into El Niño and La Niña composites and studying the delayed response of precipitation to SST forcing in four regions of Central and South America.

In this paper we concentrate on seasonal mean timescales. We find that RCA accurately simulates the main features of the precipitation climatology over the four regions and also reproduces the majority of the documented regional responses to ENSO forcing. Furthermore, the model captures the variability in precipitation anomalies between different ENSO events. The model exhibits a wet bias over the Northern Amazon and slightly over-estimates the magnitude of ENSO anomalies over Central America.

## 1.1 Introduction

The branch of climate prediction known as seasonal forecasting fills a gap between short-range weather forecasting and climate prediction. Seasonal forecasting aims to make useful predictions of climate anomalies on timescales of about one month to one year. The benefits of seasonal prediction are multiple, ranging from disaster prevention (floods and droughts) to resource planning (agriculture and energy). Past studies have established a potential predictive skill on seasonal timescales in tropical regions (Goddard et al., 2001, and references therein). The main source of this predictability stems from forcing of large scale atmospheric circulation anomalies by tropical sea surface temperature (SST) anomalies. These SST anomalies (SSTAs) evolve on relatively slow timescales, increasing atmospheric predictability beyond that normally associated with unforced atmospheric motions (Shukla, 1998). The coupled ocean-atmosphere phenomenon known as the El Niño/Southern Oscillation (ENSO) is the leading mode of interannual SST variability in the tropics (Wang et al., 1999), hence SSTAs associated with ENSO constitute a major source of potential predictability on seasonal timescales, particularly in tropical regions (Goddard et al., 2001).

Coupled Ocean-Atmosphere General Circulation Models (CGCMs) can simulate with reasonable accuracy the evolution of tropical SSTAs on seasonal timescales associated with ENSO (Latif et al., 1998; Palmer et al., 2004). Atmosphere only GCMs (AGCMs) can then be forced either with these predicted SSTAs, or with persisted observed SSTAs, in order to assess their impact on important meteorological variables. AGCMs have some skill in simulating the response of the large scale tropical atmospheric circulation to anomalous SST forcing (Philander, 1990; Shukla et al., 2000). Nevertheless, users of seasonal predictions often require localized information on regional climate anomalies, hence some means of downscaling GCM simulated large scale anomalies is required, to maximize the utility of these seasonal forecasts. Regional Climate Models (RCMs), through their increased resolution, offer one means of downscaling GCM seasonal predictions to the scale more suited to end-users (Sun et al., 2006).

This study covers areas of the tropical Americas such as Mexico, Central America, the Caribbean and northern South America as well as the tropical east Pacific and north Atlantic oceans (see Figure 1.1). A number of studies have linked east Pacific and tropical Atlantic SST anomalies to precipitation anomalies in the Caribbean and northern South America (Goddard et al., 2001). The tropical North Atlantic SST anomalies are due to both ENSO teleconnections and local variability and the relative contribution to precipitation variability of these two water basins is somewhat difficult to ascertain (Enfield et Alfaró, 1999; Giannini et al., 2000; Taylor et al., 2002). Over Mexico and Central America, the response to anomalous SST forcing is somewhat weaker than over South America yet clearly present (Ropelewski et Halpert, 1987; Enfield, 1996; Enfield et Mayer, 1997; Giannini et al., 2000; Magaña et al., 2003).

Over South America, a GCM has been used successfully by CPTEC for operational seasonal prediction over South America (Marengo et al., 2003) for a number of years. The use of RCMs (RegCM3 and EtaClim) has indicated an improvement in seasonal prediction of precipitation in regions of Brazil, such as the Amazon (Chou et al., 2005) and Nordeste (Sun et al., 2006), as a result of dynamical downscaling. In other studies, the same RCMs provide a fairly accurate simulation of precipitation over South America, both in terms of the mean climatology and anomalies during ENSO events (Fernandez et al., 2006a,b; Seth et al., 2007). Existing RCM studies covering Central America and the Caribbean are scarce. In Xie et al. (2007) the ROAM regional ocean—atmosphere model reproduces the main climatological features of the tropical east Pacific and shows an improvement in the simulation of mesoscale features due to its increased resolution. A study by Hernandez et al. (2006) describes a simulation using the MM5 RCM over Central America. Variables such as temperature, wind speed and water vapor mixing ratio were well simulated, but discrepancies in simulated precipitation were attributed to the use of only two seasonal maps of land cover. The North American monsoon (also defined as the Mexican Monsoon) described in (Adams et Comrie, 1997), is centered over northwestern Mexico and has been covered by numerous RCM studies. The MM5 RCM can reproduce the climatological features of the North American monsoon (Xu

et al., 2004) and sensitivity tests to convective schemes indicate improved performance using the Kain-Fritsch scheme (Gochis et al., 2002).

In this set of experiments we use a RCM to downscale so-called perfect boundary conditions as defined by European Centre for Medium-Range Weather Forecasts (ECMWF) analysed lateral and surface boundary conditions. This is done to assess the ability of a RCM to generate small scale regional detail with respect to ENSO forced anomalies, given accurate large scale forcing. Subsequent to a successful evaluation of the RCM downscaling ability forced by analysed boundaries, the logical next step is to force the same RCM with boundary conditions derived from an atmospheric or coupled GCM. This step is deferred to a future study. In this study we run the Rossby Center Regional Atmospheric Model version 3 (referred to as RCA) (Jones et al., 2004; Kjellström et al., 2005), with observed SSTs and analysed lateral boundary conditions (LBCs) for the period 1979 to 2005. The model was configured to cover the tropical east Pacific and tropical Americas and run at a resolution of  $0.33^\circ$  for most of our analysis. As  $0.33^\circ$  is significantly higher resolution than is generally employed by GCMs in seasonal prediction, we would also like to more directly assess the benefits of increased resolution with respect to simulating ENSO precipitation variability. To achieve this we have conducted an additional set of experiments using the same RCA model at a resolution of  $1^\circ$ , the approximate resolution of both the ECMWF analysis and operational GCMs currently in use for seasonal prediction. Comparison between the RCA  $0.33^\circ$  and  $1^\circ$  integrations will indicate benefits accruing directly from improved resolution. Figure 1.1 shows the entire model domain, while the inner dashed box shows the area of analysis (excluding the outer 15 points of the model). An assessment is made of the model's ability to simulate regional scale anomalies associated with either El Niño or La Niña conditions. This paper looks at regional-scale variability associated with ENSO at seasonal mean timescales. Our primary emphasis is on precipitation anomalies as these have the largest impact on society. Part II of this study (Tourigny et Jones, 2008b), hereafter referred to as TJ2008b, looks at subseasonal timescale precipitation.

## 1.2 Model and data

### 1.2.1 Domain of study and regions

The domain of study comprises Central America and most of the tropical regions of the Americas. The RCM domain includes the main area of the east Pacific Inter Tropical Convergence Zone (ITCZ). Convective anomalies over this region, associated with ENSO SST variability, are the main forcing term of large scale atmospheric circulation anomalies that subsequently influence Central and South America. Hence the majority of the anomalous atmospheric convection over the equatorial east Pacific and associated circulation anomalies are simulated within the RCM domain. The strong surface forcing in equatorial regions along with the relatively large model domain mean the RCM is less strongly constrained by the lateral (atmospheric) LBCs than in typical mid-latitude RCM integrations.

Referring to Figure 1.1, the regions where we evaluate the model's ability to simulate regional scale climate anomalies are : MEX (northern Mexico, 25°-30°N, 110°W-97°W), CAR (Caribbean, 5°N-25°N, 90°W-60°W), CAM (Central America, 7°N-18°N, 92°W-78°W) and NAMZ (northern Amazon, 5°S-5°N, 70°W-55°W). These regions have been chosen based on previous studies which identify regions of ENSO-related precipitation variability. Details of the observed precipitation associated with ENSO variability and the mechanisms forcing this variability, as well as relevant references, are discussed in section 1.4.1.

### 1.2.2 Model setup

RCA uses the Kain-Fritsch convection scheme (Kain et Fritsch, 1990, 1993; Kain, 2004) for representing both deep and shallow convection. Deep convection uses a CAPE consumption closure, while shallow convection is assumed to consume sub-cloud layer turbulent kinetic energy (TKE) within a given time period (Deng et al., 2003). Isotropic subgrid scale turbulence is represented by a moist TKE scheme (Cuxart et al.,

2000; Lenderink et al. (2004). Resolved scale clouds are parameterised following the approach of Xu et al. (1996), while a diagnostic shallow cumulus cloud fraction follows Albrecht (1981). A cloud fraction associated with parameterised deep convective up and downdrafts is diagnosed as a function of the convective mass-flux, following Xu et al. (1991). Large scale condensation uses the scheme due to Rasch et al. (1998), while the RCA radiation scheme is described in Savijärvi (1990) and Räisänen et al. (2000). The land surface is comprised of three active soil layers and is documented in Samuelsson et al. (2006). Surface and subsurface physiography is prescribed each month using the high-resolution ECOCLIMAP global dataset (Masson et al., 2003), which provides monthly climatological values. The model uses the Davies (1976) boundary relaxation technique with an 8 point relaxation zone for adjusting the interior RCM solution towards the prescribed lateral values.

Initial and lateral boundary conditions were obtained from observed SSTs and ECMWF ERA-40 reanalyses (Uppala et al., 2005). After August 2002 LBCs were derived from the ECMWF operational analysis. For all years covering the period 1979 to 2005, RCA is run for one calendar year with observed SSTs and analysed lateral boundary conditions (LBCs). Soil temperature and moisture values are initialized from the ECMWF analysed values relevant for the calendar month (December) of each year used as initial conditions. While we recognize that deep soil moisture spins up on much longer timescales than 13 months, the procedure employed here is done to mimic actual seasonal forecasting using a quasi-observed soil moisture field and in terms of computational cost. Experiments on soil moisture reinitialization show that frequent reinitialization increases short-term (on the order of weeks) accuracy (Qian et al., 2003), and suggest a minimal importance of soil moisture memory (Pan et al., 1999). Moreover, continuous reinitialization removes possible drift in soil moisture due to systematic errors in the RCM formulation (Qian et al., 2003).

In this study we employ only one RCM integration, per 13 month period, to define the simulated precipitation for that year. In a true GCM-RCM prediction system an

ensemble of GCM simulated LBCs would be required to better quantify the statistical robustness of any RCM simulated precipitation anomalies. In this manner, variability in the simulated LBCs (both with respect to differing GCMs and the natural variability as simulated by a single GCM) would be included in the final estimate of GCM-RCM precipitation anomalies. Here we use a hindcast approach, with analysed LBCs applied to the RCM. This we believe reduces the need to sample a variety of LBCs, although we recognize that a similar exercise with another global re-analysis data set might help to strengthen this assertion. Unfortunately this level of computation was beyond the scope of this study and must be deferred to later efforts. Similarly, for a true GCM-RCM prediction system a variety of RCMs would allow a better estimate of the statistical robustness of simulated regional responses to a given LBC dataset. Again application of a suite of RCMs is beyond the scope of this study.

The final step in establishing the statistical robustness of RCM precipitation anomalies is to ask, for a given LBC dataset and RCM what is the RCM internal variability on 3-12 month lead times? To assess this we constructed a five member ensemble of RCA simulations for the El Niño year of 1983, whereby RCA was initialized progressively one day later in the period December 1 to 5 of 1982. Each RCA simulation used the same LBC and SST dataset and was run to the end of December 1983. Analysis of the simulated precipitation in this five member ensemble indicated the major regional scale anomalies were very similar across all members, suggesting the control exerted by the (anomalous) SST and large-scale atmospheric circulation, as defined by the applied LBCs, limits the degree of variability internal to the RCM domain. This argument holds most strongly for the stronger ENSO events which are the main emphasis of this work.

### 1.2.3 Observations

The emphasis of this study is on precipitation variability due to its large societal impact. Sea level pressure (SLP), low-level (925 hPa) wind, as well as upper-level (250hPa) geopotential height and wind are also studied to better understand the dynamics of

the atmospheric circulation anomalies controlling the regional patterns of anomalous precipitation.

Satellite observations offer the most spatially and temporally complete estimate of observed precipitation. The highest resolution observation is the Tropical Rainfall Measuring Mission (TRMM) product 3B43 (Huffman et al., 2007), available at a resolution of  $0.25^\circ$  and derived from satellite and in-situ observations. TRMM 3B43 is only available from 1998 to present, this period does not include a sufficient number of ENSO events for a robust analysis of the simulated ENSO forced variability. Version 2 of the Global Precipitation Climatology Project (GPCPv2) gives monthly estimates of precipitation on a grid of  $2.5^\circ$  resolution, from 1979 to present (Adler et al., 2003). These observations are at a coarser resolution than the model ( $2.5^\circ$  vs.  $0.33^\circ$ ), therefore a more precise gridded product is required for land areas. We choose the Climatic Research Unit's TS 2.1  $0.5^\circ$  global land dataset, covering the period 1901-2002 (Mitchell et Jones, 2005). An additional quasi-observation is given by the ECMWF ERA-40 re-analysis available for 1957-2002, as well as ECMWF operational analysis from August 2002, from which we obtain precipitation, SLP, geopotential height and wind vector estimates. The resolution of ERA-40 and ECMWF is T106 ( $\sim 1^\circ$  at the Equator), although all variables excluding precipitation were obtained at  $2.5^\circ$  resolution. The reader is reminded that ECMWF is also used as a LBC for the regional model, allowing an estimate of the "added value" of the RCM compared to the driving data set. We refer to these datasets respectively as TRMM, GPCP, CRU and ECMWF. From these datasets we evaluate the model's climatology and interannual variability for the 1979-2001 period. TRMM is used to evaluate the model performance for the 1998-2005 period, with an emphasis on high resolution regional patterns. In particular we focus on regional scale, seasonal mean precipitation anomalies associated with El Niño and La Niña conditions.

## 1.3 Climatology

### 1.3.1 Methodology

The first step in our evaluation is to assess the simulated precipitation climatology over the regions of interest. While in principle interannual anomalies associated with ENSO can still be simulated by a model that fails to accurately simulate the regional climatology, the propagation and development of remote ENSO teleconnections is often sensitive to details of the background climatology (Simmons et al., 1983; Sardeshmukh et Hoskins, 1988). Furthermore, an accurate representation of the climatological conditions increases our confidence that the model correctly simulates key regional climate processes. We first evaluate the seasonal mean SLP and precipitation, concentrating on the boreal winter (JFM) and summer (JAS) seasons. Secondly we plot annual cycle time series of spatially averaged precipitation, for land points only, for each of the regions shown in Figure 1.1.

### 1.3.2 Results

#### 1.3.2.1 Seasonal Averages

Figure 1.2 shows the climatological mean SLP and 925 hPa winds (left column) and 250 hPa geopotential height and winds (right column) for seasons JFM and JAS (averaged for 1979-2001) from ECMWF and RCA. Figure 1.3 gives the climatological seasonal mean precipitation for the same seasons and period, here GPCP, CRU, ECMWF and RCA are presented.

Season JFM (Figures 1.2a-d and 1.3 left column) shows a relative minima in observed precipitation on the equator in the east Pacific ITCZ, which is mainly captured by the model, with a small positive bias compared to GPCP. The minima simulated over northern South America is realistic, although the maxima in the southern Amazon and the Atlantic ITCZ are somewhat excessive. ECMWF is excessive over most of the domain

except over the southern Amazon, where precipitation is underestimated. It is worth noting that the excessive precipitation simulated by RCA close to its eastern boundary in the Atlantic ITCZ is also evident in the ECMWF results. This may suggest a strong and perhaps erroneous forcing of the RCA precipitation by the adjacent ECMWF atmospheric boundary conditions. Upper-level geopotential and wind vectors show a maximum in geopotential height over the southern portion of the RCA domain and the presence of the subtropical jet over the northern portion of the domain, accurately simulated by RCA.

Over the Amazon region in JFM season, the low level wind field in RCA is clearly stronger than in ECMWF (Figure 1.2a,c). This stronger wind field is consistent with the higher rainfall rates in RCA over the Amazon region during JFM compared to ECMWF (Figure 1.3e,g). We are unable to determine if the excessive precipitation in RCA (and associated diabatic heating) causes the excessive low level wind speeds in RCA, or if the wind speed bias and associated convergence of moisture into Amazonia drives an erroneous response in the convection scheme. Compared to GPCP and CRU observations, the RCA precipitation is excessive in this region while ECMWF precipitation is biased low. We are unable to evaluate the accuracy of the ECMWF low level winds in this region, but through a balanced thermal-dynamics argument one might conclude that the “true” low-level wind speed is therefore somewhere between the ECMWF and RCA values.

In season JAS (Figures 1.2e-h and 1.3 right column), GPCP precipitation and ECMWF SLP and winds indicate the ITCZ has migrated to  $\approx 10^\circ\text{N}$  in the eastern Pacific and western Atlantic, with a significant strengthening of the east Pacific ITCZ. This migration and intensification, accompanied by a northward-displacement of maximum 250 hPa geopotential height, is largely captured by the model. A clear coastal precipitation minimum is correctly simulated by RCA along the west coast of South America in JAS, while precipitation rates associated with the North American Monsoon are also accurate, with the Mexican monsoon penetrating to  $\approx 27^\circ\text{N}$  along the west coast. The main

area of disagreement lies in the more rapid decrease in precipitation in the observations as one moves south of the Amazon region in South America. RCA simulates a number of regional precipitation patterns that are spatially supported by the CRU observations. In this region the actual observation data going into the CRU dataset is uncertain and may not be actually representative of  $0.5^\circ$  resolution. Hence it is difficult to evaluate the simulated regional details without an improved observational dataset. RCA reproduces most of the spatial structure of precipitation in JAS, although of higher intensity in some areas. In section 1.5 we will show that this higher intensity is comparable to the higher-resolution TRMM data.

Regions of high SLP over the oceans generally correspond to the descending branches of the Hadley Cell and are coincident with extreme dry conditions. In RCA the SLP field is well structured with the minimum SLP well located and a clear northward extension of the ITCZ in JAS into Mexico, coincident with the North American monsoon. SLP values over the Atlantic and South America are also generally accurate. There is, however, a positive SLP bias of  $\approx 1$  hPa in the east Pacific, particularly in the ITCZ region. The ECMWF climatological precipitation for JAS shows a clear overestimate in the Pacific ITCZ. In the tropics, diabatic heating associated with precipitation and surface SLP are dynamically related. In a free-running model (i.e. one not constrained by the assimilation of observations), a positive precipitation bias such as in ECMWF might be expected to be associated with a low pressure bias in the ITCZ. In ECMWF this relationship is not necessarily present, as the assimilation of SLP observations can bring the analysed SLP back towards observed values even while the atmospheric diabatic heating is overestimated. To partially evaluate the ECMWF SLP field we also analysed SLP and precipitation from the Japanese Reanalysis (JRA25; Onogi et al., 2007). The JRA25 precipitation values in the east Pacific ITCZ are less than in ECMWF (although still higher than satellite values), but the JRA25 and ECMWF SLP fields are quite similar (not shown). We therefore conclude that the assimilation process likely constrains SLP in ECMWF and the RCA  $\approx 1$  hPa bias is a genuine model error.

### 1.3.2.2 Annual Cycle

In Figure 1.4 we plot the climatological mean annual cycle of precipitation (years 1979-2001) for the four separate regions outlined in Figure 1.1. On the x-axis of the plots we indicate the typical rainy season duration. Figure 1.4a shows results for the CAR region, where RCA reproduces the annual cycle and seasonal transitions, mostly within the range of GPCP and CRU observations. ECMWF values are excessive in this region and cannot be used as an observational surrogate. Figure 1.4b shows the CAM region, where RCA follows the GPCP estimates quite closely. CRU and GPCP over the CAM region differ by up to 2 mm/day in the rainy season (May-October).

Close inspection of the rainy season reveals a well documented feature of precipitation in Central America : the Mid-Summer Drought (MSD), when there is a relative minima of precipitation in July-August in the middle of the rainy season (Magaña et al., 1999; Alfaro, 2002; Magaña et Caetano, 2005; Taylor et Alfaro, 2005; Small et al., 2007). RCA fails to represent this feature in the climatological spatial average over CAM. To investigate this problem further, Figure 1.5 shows the climatological average of July and August rainfall minus the average for June and September over the entire model domain. The same method is used in Small et al. (2007), wherein it is shown that the MSD is initiated by the northward migration of the east Pacific ITCZ and the westward expansion of the Atlantic subtropical high. These changes in SLP induce low-level divergence and subsidence over Central America, and the circulation changes due to the precipitation deficit induce a low-level anticyclonic flow over the Gulf of Mexico, with subsequent drying. In RCA, SLP and low-level wind changes in July, relative to June, are negligible in the Caribbean, whereas ECMWF shows increased northeasterlies and divergence (not shown), which explains the precipitation deficit in the western Caribbean (Figure 1.5c). However, both ECMWF and RCA show a precipitation deficit on the west coast of Central America (north of Costa Rica), consistent with divergence and subsidence. Moreover, all datasets agree on the dry anomaly over the Gulf of Mexico (although slightly over-estimated by RCA). The precipitation increase over western

Mexico (part of the Mexican Monsoon) is also well simulated by RCA. There is evidence, both in model and observations, of a precipitation increase on the east coast of Central America, due to the increased easterlies associated with orographic forcing. RCA does therefore appear to simulate the MSD over the western part of Central America, but incorrectly simulates a wet anomaly in the western Caribbean, as a result the MSD is absent in the spatial average of the CAM region. Nevertheless, specific land-based negative and positive anomalies in the July and August precipitation relative to the June and September amounts are well captured by RCA over central America (see Figure 1.5d). The primary problem related to the simulation of the MSD appears to be associated with an incorrect response over the west Caribbean Sea. Further analysis is required to fully understand this incorrect response.

Over the NAMZ region (Figure 1.4b) the rainy season extends from February to July and the seasonal variation is of smaller amplitude. The model is generally wetter than observed, but the timing of the rainy season is reasonably captured. Moist conditions extend too long into the OND season, with an unrealistic secondary maximum in December. This is similar to many models which produce a secondary peak in precipitation associated with the semi-annual cycle of solar forcing at the equator (Seth et al., 2007; Rauscher et al., 2007). A continuous three-year integration has shown that this is not a problem related to spin-up of soil moisture with the biannual peak in precipitation evident in all three years of this run. ECMWF precipitation intensity is closer to observations, however the amplitude of the seasonal variations is under-estimated. The MEX region (Figure 1.4c) is far drier, exhibiting a weak rainy season from May-September. The timing of the rainy season is well reproduced by the model, however there is a slight wet bias ( $\sim 1$  mm/day) during that period which is also present in ECMWF.

In this section we have shown that RCA simulates the climatological precipitation with some degree of accuracy both over the east Pacific and adjacent land regions. The model successfully captures a number of regional details, giving some confidence it simulates the majority of the important processes controlling precipitation over the

tropical Americas and eastern Pacific. A more detailed evaluation of small-scale regional precipitation details is deferred until section 1.5 where we employ the TRMM dataset for the shorter 1998-2005 period. In the next section we evaluate the simulated precipitation variability in response to prescribed ENSO SST forcing.

## 1.4 Interannual variability

### 1.4.1 A review of ENSO effects and teleconnections

During the warm phase of ENSO (El Niño), anomalously warm waters are located in the central and east Pacific with a general weakening of the climatological east-west SST gradient. In the cold phase of ENSO (La Niña), central and east Pacific SSTs are anomalously cold with a concomitant increase in the longitudinal SST gradient. In El Niño events, warm SSTAs lead to anomalous deep convection in the central and east Pacific (Philander, 1990). Through atmospheric and oceanic teleconnections, other regions of the globe experience anomalies in rainfall and temperatures in response to this anomalous Pacific convection (Alexander et al., 2002). Studies by Ropelewski et Halpert (1987, 1996) identify regional scale patterns associated with El Niño (warm ENSO) events through the study of composites representing years (-), (0), and (+), which are the years before, during and after a “typical” ENSO event, with the peak of anomalous SST in the OND(0) season (i.e. October-December of year (0)).

Anomalous precipitation patterns documented over our domain of study associated with El Niño conditions are ; 1) wet anomalies over the Gulf of Mexico and northern Mexico from October (0)-March (+); 2) dry conditions over Central America and the Caribbean from July-October (0); 3) dry conditions over northeastern South America from July (0)-March (+). The regional patterns for La Niña are, in a general sense, opposite signed anomalies to El Niño (Aceituno, 1988; Ropelewski et Halpert, 1989), therefore subsequent analysis will concentrate on the warm El Niño events, with some minor verification that the model simulates correctly the opposite signed La Niña anomalies.

The mechanisms thought to induce precipitation anomalies related to El Niño are multiple. During the summer of year (0), as the SST anomaly is becoming established, anomalous convection over the east Pacific modifies the Walker and Hadley circulations, with increased subsidence and decreased rainfall in the Caribbean (Chiang et al., 2000). The reduction in SLP over the tropical east Pacific and increase over the North Atlantic (which strengthens the trade winds) implies low-level divergence over the Caribbean Sea and convergence in the tropical east Pacific. This is responsible for a decrease in moisture convergence, and thus precipitation, over Central America and the Caribbean (Giannini et al., 2000, 2001b). The anomalous Walker Cell is also thought to be responsible for increased subsidence and decreased rainfall over the Amazon and northeast Brazil (Kousky et al., 1984).

A chain of teleconnections known as the “Atmospheric Bridge” (Alexander et al., 2002) is thought to regulate the delayed responses to ENSO throughout much of the study area. Anomalous tropospheric heating causes a disturbance to the PNA (Pacific/North American) pattern which brings lower SLP and increased precipitation around the Gulf of Mexico in the winter season of year (+) (Horel et Wallace, 1981; Giannini et al., 2001b). Concurrently, the PNA anomaly is also responsible for a decrease in the North Atlantic trade winds, through a weakening of the Atlantic subtropical High (Nobre et Shukla, 1996). One consequence of this is reduced moisture convergence into the Amazon basin in spring (+), leading to decreased convection (Marengo, 1992; Marengo et Hastenrath, 1993) and a delay in the onset of the rainy season over the northern Amazon (Liebmann et Marengo, 2001; Marengo et al., 2001). Another consequence of the decreased trade winds is a warming of the tropical North Atlantic (TNA), leading to an increase in precipitation in spring (+) over the Caribbean (Giannini et al., 2001b; Enfield et Mayer, 1997). However, a higher than average NAO (North Atlantic Oscillation) in the 1980s and 1990s (during our period of study), strengthening the Atlantic trade winds, is thought to have attenuated or canceled these effects (Giannini et al., 2001a).

### 1.4.2 Methodology

To assess RCA's ability to represent key regional anomalies associated with the aforementioned ENSO variability, we follow Ropelewski et Halpert (1987) and develop composite ENSO events for years (0) and (+). We do not consider the years (-) as there are no documented impacts during this period over our regions of interest. We calculate monthly El Niño and La Niña composites for selected years within our period of study, which results in composites Niño (0), Niño (+), Niña (0) and Niña (+). The resulting metrics are thus defined as :

$$NINO A = \overline{NINO} - CLIM \quad (1.1)$$

$$NINA A = \overline{NINA} - CLIM \quad (1.2)$$

where  $\overline{NINO}$  and  $\overline{NINA}$  are the basic ENSO composite values of a given variable for a given month,  $CLIM$  is the climatological average of the same variable for the same month and  $NINO A$  and  $NINA A$  are the anomalies of the ENSO composites.

The events chosen for composite means are the ones used by Seth et al. (2007), based on the National Oceanic and Atmospheric Administration (NOAA) Climate Prediction Center's Oceanic Niño Index (ONI). The condition for defining an El Niño (warm) or La Niña (cold) event is a SST anomaly of  $\pm 0.5^\circ\text{C}$  relative to the 1971-2000 base period, over the Niño 3.4 region for five overlapping seasons, using the ERSST.v2 dataset (Smith et Reynolds, 2004). We choose only the strongest ENSO events in order to obtain a clear anomaly signal. The relatively mild La Niña of 1984-1985 has been excluded because the precipitation anomalies are opposed to other La Niña events in the NAMZ and MEX regions. Figure 1.10d shows the corresponding SST anomalies and Table 1.1 gives the strong ENSO events with corresponding years (0) and (+).

We first analyze spatial maps of SLP, 925 hPa wind, geopotential height and wind at 250 hPa and precipitation anomalies for seasons JAS(0) and JFM(+) to evaluate the simulated large-scale anomalies. Secondly we plot annual cycle time series of spatially

averaged precipitation anomalies over the land points of each of the chosen regions (CAR, CAM, NAMZ and MEX) to verify if the known regional anomalies are accurately simulated. We apply a 3-month running mean to the monthly anomalies to highlight seasonal timescales. A final analysis of precipitation variability is done using a multi-year time series of spatially meaned anomalies, to determine if the model reproduces regional variability associated with different ENSO events.

### 1.4.3 Results

#### 1.4.3.1 Seasonal Averages

The important periods of precipitation anomalies associated with ENSO are respectively July-October (0) for CAR and CAM, July (0)-March (+) for NAMZ and October (0)-March (+) for MEX (see section 1.4.1). The following section deals only with seasons JAS(0) and JFM(+) which capture the majority of these anomaly periods. Figure 1.6 shows the NINOA for SLP and 925 hPa wind and 250 hPa geopotential height and wind field, for both ECMWF and RCA. To show the impact on precipitation we plot the El Niño anomalies (NINOA) for GPCP, CRU, ECMWF and RCA in Figure 1.7.

For composite El Niño conditions JAS(0) is when warm SST anomalies first appear in the eastern tropical Pacific, while there is a weak cold anomaly in the tropical North Atlantic. The model responds accordingly, with anomalous low pressure and convergence (Figure 1.6c) in the lower levels and increased convection and precipitation (Figure 1.7g) over the area of positive SSTAs (eastern tropical Pacific), in general accordance with ECMWF SLP and wind anomalies and GPCP precipitation. This anomalous convection modifies the position of the Walker Cell and strengthens the local Hadley Cell, causing increased subsidence over the Caribbean, Mexico and northern South America, east of the Andes. This can be seen in the upper levels through anomalies in the geopotential height (positive over the eastern tropical Pacific and negative over the Caribbean) and anomalous westerly upper-level winds at the equator. The resulting dry anomaly over northeast South America is correctly simulated (Figure 1.7g).

ECMWF SLP anomalies indicate weak anticyclonic anomalies both east and west of Mexico in JAS(0), which reduces moisture convergence over the continent and onto the east and southwest coasts of Mexico. JAS(0) precipitation anomalies in this region (Caribbean and Mexico), while of the correct sign, are excessively dry in RCA (mostly over the Gulf of Mexico as seen in Figure 1.7 left column). The corresponding SLP and low-level wind field anomalies in RCA are also slightly more intense than seen in ECMWF, consistent with an excess decrease in low-level moisture convergence (and precipitation) over these areas. Furthermore, the 250 hPa geopotential height anomalies in RCA are excessive and displaced somewhat to the west. It appears that the Kain-Fritsch convection scheme in RCA is too responsive to anomalous subsidence in this region, which is part of the descending branch of the Hadley Cell. In this region of anomalous subsidence, model convection appears to completely shut down, whereas in reality it is likely that sporadic weak convection still occurs. As a result the simulated negative precipitation anomaly is larger than observed.

Season JFM(+) is when the PNA (Pacific/North American) pattern disturbance – initiated in the OND(0) season – spreads southeastward, influencing most of the northern part of the domain, with anomalously low SLP values. Wind patterns shift dramatically (Figure 1.6e,g), with reduced Atlantic easterly trade winds, leading to reduced evaporation and relatively warmer SSTs over the Caribbean. The PNA anomaly can be clearly seen in the negative 250 hPa geopotential height anomalies (Figure 1.6f,h) and strengthening of the subtropical jet in the northern portion of the RCA domain in JFM(+) and are in very good agreement with ECMWF anomalies. A widespread wet anomaly north of  $\approx 20^\circ\text{N}$  is well captured in the model (Figure 1.7 right column) and linked to the southward influence of the PNA forcing. Over Central America the RCA simulated negative anomalies are comparable to observations. Most of South America in the model domain is under the influence of decreased easterlies which reduces moisture convergence leading to a dry precipitation anomaly in both the observations and model, whereas ECMWF precipitation suggests a widespread wet anomaly. In JFM(+) season the CRU observations indicate a thin positive precipitation anomaly along the coast of

Ecuador, Peru and northern Chile. This small scale feature is reasonably captured in the RCA results.

In this section we discuss La Niña precipitation anomalies (NINAA), for seasons JAS(0) and JFM(+), shown in Figure 1.8. This is done to verify if the model can simulate the opposite signed precipitation anomalies associated with La Niña SSTAs. Figure 1.8a,e indicates a weaker east Pacific ITCZ in JAS(0) accompanied by a weaker descending branch of the Hadley Cell over the Caribbean, and of the Walker Circulation over northeastern South America. This results in positive precipitation anomalies in these two regions in JAS(0), both of which are relatively well captured by RCA. Wet anomalies in the Caribbean are of comparable magnitude in RCA compared to observations. The MEX region and Gulf of Mexico are excessively wet in RCA in season JAS(0), analogous, in a reverse sense, to the excessive dryness in season JAS(0) of the El Niño composites (Figure 1.7g). Here the convection scheme may be too responsive to reduced climatological subsidence, triggering excessively strong convection in an environment only slightly more supportive of convection. The South American continent is well simulated, with dry conditions south of 5°S and wet conditions to the north.

In season JFM(+) the model underestimates a dry anomaly along the east Pacific ITCZ. Dry conditions prevail over most of Mexico and the Gulf of Mexico (the reverse of PNA-induced wet conditions in the El Niño composites) and are generally well simulated (note that the absolute magnitude of the anomaly is very small). The Caribbean Sea and tropical North Atlantic are under the influence of a PNA-induced high pressure anomaly in JFM(+) which causes an increase of the easterly trade winds, with an increase in moisture convergence and precipitation over the Amazon (Marengo, 1992). RCA generally simulates this increase in precipitation over northeast South America. As in the El Niño JAS(+) anomalies, ECMWF shows opposite signed anomalies to those observed in some parts of South America. It is worth noting that RCA receives its LBCs from the ERA-40/ECMWF analysis. Hence this improvement in the precipitation anomaly field should be seen as a clear local improvement through dynamical downscaling.

### 1.4.3.2 Annual Cycle

To assess the time evolution of simulated ENSO anomalies over the four regions of interest we present, in Figure 1.9, three-month running mean time series of precipitation anomalies separately for El Niño (left column) and La Niña (right column) composite conditions (obtained as averages across the years given in Table 1.1). On the x-axis of the figures we indicate the generally accepted time periods, within the annual cycle, of El Niño and La Niña forced precipitation anomalies (dry/wet) over each region.

In CAM (*typically dry/wet anomalies for El Niño/La Niña composites from July-October (0)*) RCA correctly simulates a dry anomaly from May (0)-May (+) in the El Niño composite (although of slightly excessive magnitude in May-June (0)). A similar, reverse behavior is seen in the La Niña composites. After November (0) the agreement between all datasets becomes weaker, particularly for the La Niña composites where the anomalies are small and RCA is not able to match observations. It should be borne in mind that there are no consistent and documented ENSO forced anomalies in this period and region. In the broader CAR region (*typically dry/wet from July-October (0)*), the dry anomaly from May (0)-March (+) under El Niño conditions is well simulated in RCA, with a slight dry bias from January-July (+). In the La Niña composites the simulations are generally of opposite sign to the El Niño anomalies and are accurately simulated until February (+), after which none of the four data sets agree on the anomaly sign.

Over the NAMZ region (*typically dry/wet from July-March (0)*) El Niño conditions are associated with dry anomalies throughout most of the two year composite. As early as May (0) there are dry anomalies (the strongest anomalies being in December (0)-February (+)), and the model is nearly always within the observational range. The ECMWF precipitation fails completely to capture the negative anomaly over NAMZ. As the rainy season in the northern Amazon is normally from February to July, this dry anomaly in El Niño years can be associated with a delay in the onset of the rainy season in year (+). This has been confirmed in a number of earlier studies (Liebmann et Marengo, 2001; Marengo et al., 2001) and will be addressed in TJ2008b using pentad

precipitation data. The La Niña composites show practically the opposite anomaly structure to El Niño conditions, with prevailing wet anomalies peaking in January-February (+). This anomaly pattern is also extremely accurate in the RCA results, with the ECMWF anomaly again being an outlier. Analogous to El Niño composites, this wet anomaly is associated with an early onset of the rainy season.

The MEX region (*typically wet/dry from October (0)-March (+)*) is primarily influenced by the PNA pattern. The El Niño composites show a wet anomaly from November (0)-April (+) in the observations. The dry bias in the model in this region results in a weaker and shorter wet period than observed. After this wet period the observations disagree and there is no documented ENSO anomaly pattern. The La Niña composite anomalies are of smaller magnitude in the winter. RCA exhibits excessive magnitude of both the El Niño (negative) and La Niña (positive) anomalies over MEX, consistent with the excessive dry/wet anomalies respectively discussed in the previous section.

#### 1.4.3.3 Seasonal anomaly time series

In order to evaluate the simulated variability between different ENSO events we plot in Figure 1.10 a time series of precipitation anomalies over land for all years. For the regions CAR, NAMZ and MEX we show the interannual variability of precipitation for a single season. The selected seasons (*JAS for CAR and JFM for NAMZ and MEX*) are chosen based on the seasons of largest anomalies in the ENSO composites. Figure 1.10d shows three month running mean anomalies of the ERSST.v2 dataset in the Niño 3.4 region, with base climatology from 1971-2000 and identifies the ENSO events (El Niño in light grey, La Niña in dark grey).

The response in precipitation anomalies is not a simple function of the magnitude of SST anomalies in the tropical east Pacific. Moreover, regional consequences of ENSO are not always consistent with “canonical” ENSO events (represented by the composites), in accordance with results from Sardeshmukh et al. (2000). As an example, in the 1984-1985 La Niña event, conditions in JFM(+) are contrary to the composite La Niña

anomalies (e.g. dry in NAMZ where the composites show wet). In addition, the 1997-1998 El Niño does not conform to the composite anomalies in the MEX region, while it is very representative in other areas. The model generally agrees with observations and captures the variability between the different ENSO events across the different regions. ECMWF is a clear outlier in regions CAR and NAMZ.

Linear correlations (Pearson correlation coefficient) in time between RCA and the two observational time series are shown in Table 1.2, for all years and for strong ENSO years only (defined in 1.1). The MEX region is particularly well correlated for all years, whereas in the CAM region correlation is the lowest and generally not statistically significant. Correlations between RCA and ECMWF are much lower (except in MEX) and are not shown. The correlation for the strong ENSO years is higher than for all years and is greater than 90% in all regions except CAM. This indicates increased predictability during years of strong ENSO forcing. In order to assess the added value of dynamical downscaling we also show the correlation between ECMWF and the observations. The correlations are smaller or very close to those between RCA and the observations, except in MEX where more observational data is likely included in the assimilation process of ECMWF. We conclude that where there a relatively small amount of local data included in the ECMWF assimilation system, RCA has a better performance than ECMWF in terms of simulating year-to-year precipitation variability.

#### 1.4.3.4 Discussion

The use of composite ENSO events has allowed us to evaluate the average performance of a regional climate model in simulating regional-scale, seasonal mean anomalies associated with ENSO when forced by observed SSTs and analysed LBCs. This is a first order evaluation of the ability of a RCM to downscale large scale circulation anomalies over the tropical Americas. The model generally captures the sign of the precipitation anomalies in the important seasons, although a few regions of inaccuracy do exist. The most problematic area is the Caribbean and Gulf of Mexico in the JAS(0) season when RCA

over-estimates the El Niño related dry anomaly and conversely over-estimates the wet anomaly in this region in La Niña periods. The Kain-Fritsch convection scheme appears excessively responsive to small changes in large-scale subsidence. During (anomalous) periods of weak, large-scale subsidence (generally not supportive of deep convection), simulated convection essentially shuts down. Conversely during (anomalous) periods of weak, large-scale ascent (generally supportive of deep convection), model convection increases dramatically. We believe this binary response of model convection to changes in large-scale subsidence is much greater than in the real world and is the primary cause of the excess anomalies in this region. In the NAMZ region, the model is very accurate except for a small dry bias in January-March (+), which is just before the rainy season of year (0). This could potentially lead to errors in the prediction of the onset of the rainy season, which exhibits sensitivity to ENSO forcing. The MEX region shows a small dry bias at the end of the rainy season of year (0) and during the winter (+).

By looking at the seasonal anomalies for the different years of the integration, we have established that ; 1) there is large variability amongst different ENSO events ; 2) RCA is able to capture most of this variability ; 3) some ENSO events do not correspond to the “canonical” events as represented by the composites.

## 1.5 Assessing the benefits of increased resolution

The potential added value of using a high resolution climate model is difficult to assess, especially in tropical regions where reliable high resolution observations are scarce. In order to make a preliminary estimate of the benefits of increased model resolution we ran RCA at a lower resolution of  $1^\circ$  (named here RCA1) using the same model domain and boundary conditions. We compare both runs to GPCP and TRMM for the 1998-2005 period. The shorter time period is used in order to compare the model precipitation against the higher resolution TRMM observations. In Figure 1.11 we show the climatological average of seasons JFM and JAS. The finer detail, high intensity precipitation simulated by RCA in the Pacific ITCZ is consistent with the TRMM observations. Si-

milarly, regional scale details in precipitation associated with variable orography over South America are seen in TRMM and RCA, but are absent in the lower resolution datasets such as GPCP. When spatially averaged over a larger region GPCP and TRMM are very similar (not shown), however TRMM and RCA do both show increased detail and localized intensity maxima. Finally the lower resolution RCA1 reproduces the general spatial patterns of precipitation but shows excessive maxima (compared to the higher-resolution RCA), particularly over northern South America and regions of orographic forcing. Examination of the individual resolved and convective precipitation components (not shown) indicates the primary cause of increased precipitation in RCA1 is associated with excessive triggering of convection over the more widespread/smooth orography in RCA1. In the Rossby Center model semi-lagrangian dynamics a 1-2-1 filter is applied to the orography field in order to maintain numerical accuracy at long timesteps. This acts to extend the spatial influence of orography on the resolved dynamics in RCA1 (of lower resolution) compared to RCA (of higher resolution). Upward directed, lower tropospheric vertical velocities (as frequently simulated on the upslope of mountains in numerical models employing terrain-following coordinates) can then play an important role in allowing frequent convection in these regions through its role in the Kain-Fritsch trigger function (Kain et Fritsch, 1993).

As the 1998-2005 period is rather short and contains few ENSO events, we use a single ENSO event to assess the benefits of increased resolution in RCA with respect to downscaling regional precipitation anomalies. We show here the 1999-2000 La Niña event because it is the most “canonical” ENSO event during the available period. Figure 1.12 shows the precipitation anomaly (NINAA) during the JAS(0) and JFM(+) seasons of the said La Niña event. RCA shows increased (sub-regional) detail when compared to RCA1 and is also more accurate in several regions. Improvements in JAS(0) are seen in the Caribbean Sea (where RCA1 shows mostly positive anomalies), in northern South America (specifically east of the Andes where there are negative anomalies in the TRMM observations) and in northern Mexico. In season JFM(+), RCA shows increased accuracy in areas surrounding the northern Andes, notably a negative anomaly

on the eastern slopes is poorly captured by RCA1. Nevertheless, RCA1 does capture the majority of wet anomalies in CAR, CAM and NAMZ regions during the La Niña event. These results do suggest that a GCM run at a resolution of  $\approx 1^\circ$  could provide a reasonable amount of regional detail in support of local planning activities.

## 1.6 Conclusions

When forced by observed SSTs and analysed lateral boundary conditions RCA is able to; 1) simulate with reasonable accuracy the climatological annual cycle of precipitation over the tropical east Pacific and distinct regions of Central and South America; 2) capture most of the regional scale seasonal mean precipitation anomalies over the tropical Americas associated with ENSO forcing; 3) capture the variability between different ENSO events. Moreover, the large-scale anomalies in SLP and low-level winds that are integrally related with the precipitation anomalies, are also well represented by the model. Simulated climatological precipitation over northern Amazon exhibits a wet bias and an erroneous secondary rainfall maximum in December. Modifications to the convection scheme appear necessary to reduce an over-estimate of the precipitation anomalies in some regions (e.g. Central America), associated with an over-sensitivity to anomalous large scale vertical velocities. Nevertheless, the simulated precipitation variability related to ENSO forcing appears quite realistic and supports the use of this RCM for future studies into regional climate variability over the tropical Americas. A companion paper (TJ2008b) looks at the ability of RCA to simulate subseasonal precipitation anomalies associated with ENSO. In future work we plan to repeat this exercise forcing RCA with boundary conditions from a free running GCM. This will aid in determining the contribution of local (east Pacific) SST forcing versus more remote forcing, as defined by the RCM lateral boundary conditions, in determining interannual precipitation variability over the tropical Americas.

*Acknowledgments.*

We acknowledge the assistance of Anders Ullerstig and Patrick Samuelsson of the Rossby Center at the Swedish Meteorological and Hydrological Institute (SMHI) in preparing the lateral and surface boundary conditions used to force RCA. RCA integrations were performed at the National Supercomputer Centre in Linköping, Sweden. This research was funded by CLIVAR grant 201649, NSERC grant RGPIN/327250-2006, CFCAS grant NW CRCMD and Ouranos Inc. ECMWF ERA-40 data used in this study have been provided by ECMWF.

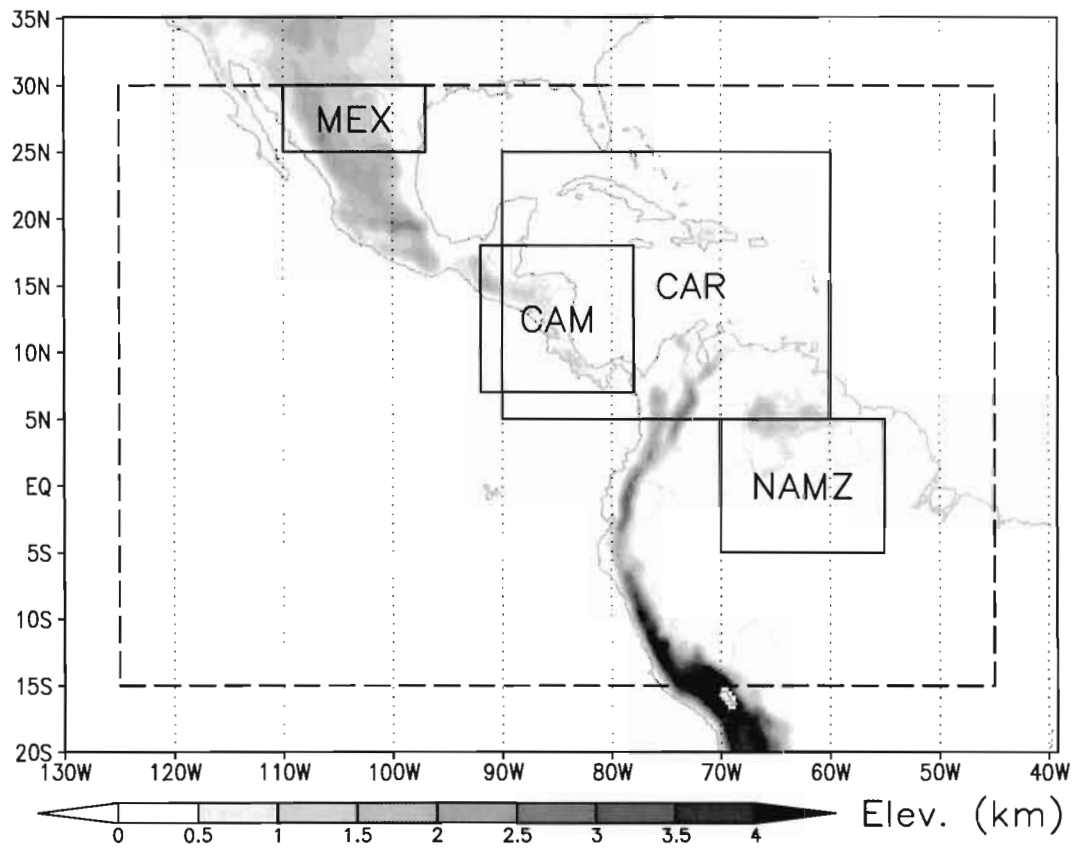


**Figure 1.1** Domain of the study and chosen regions. The dashed box shows the area of analysis.

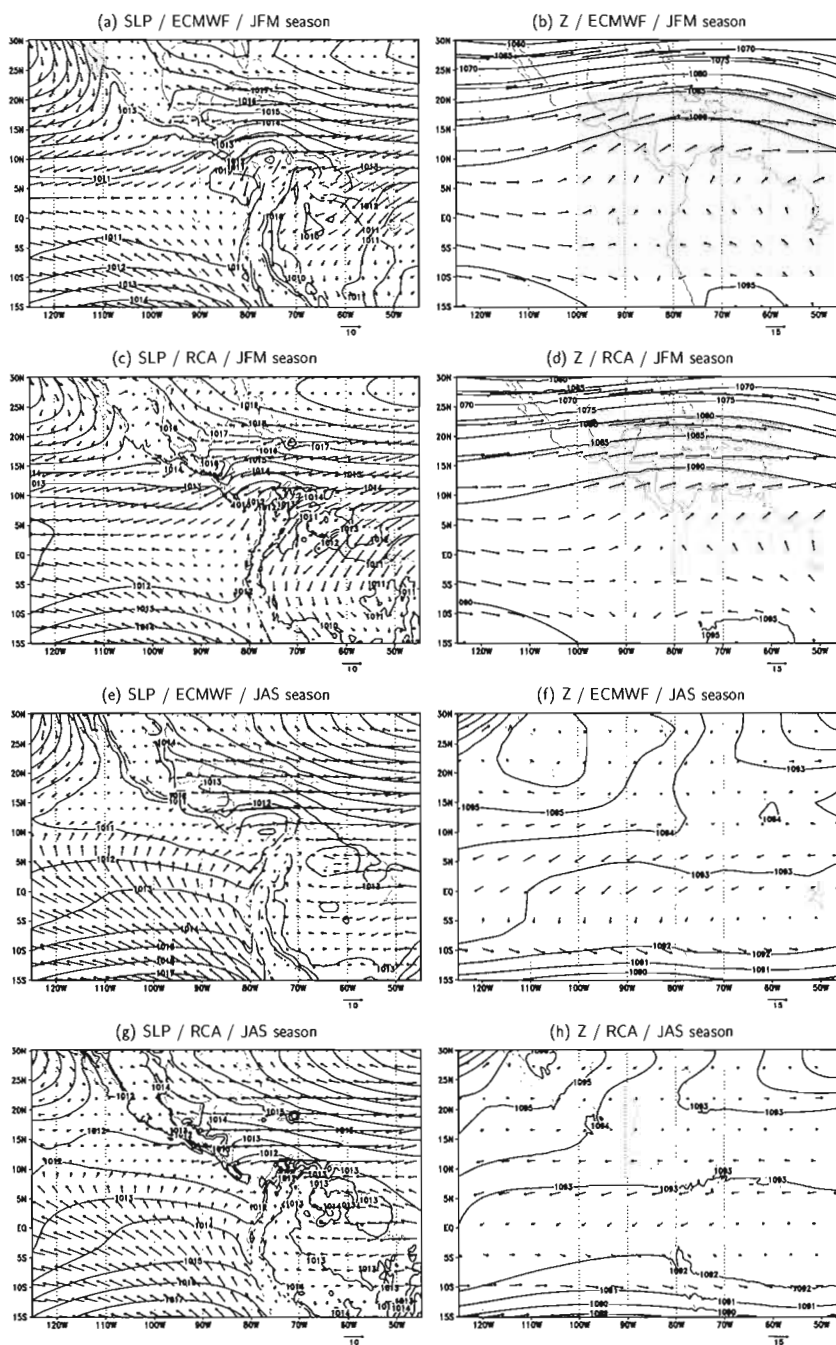


**Figure 1.2** Climatological SLP (contours in hPa) and 925 hPa winds (vectors in m/s) in left column, 250 hPa geopotential height (contours in dam) and winds (vectors in m/s) in right column. The scale of the wind vectors is indicated on each figure.

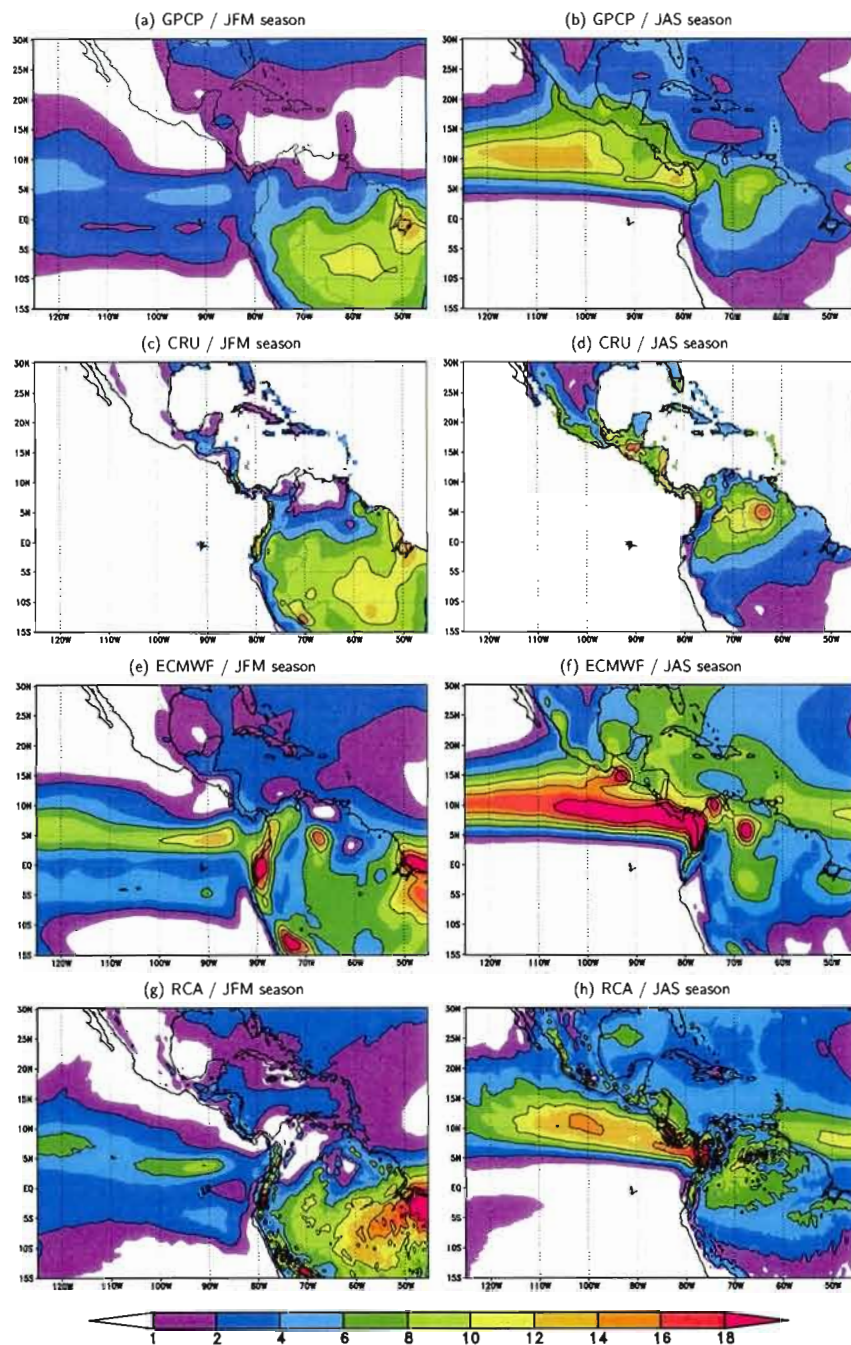
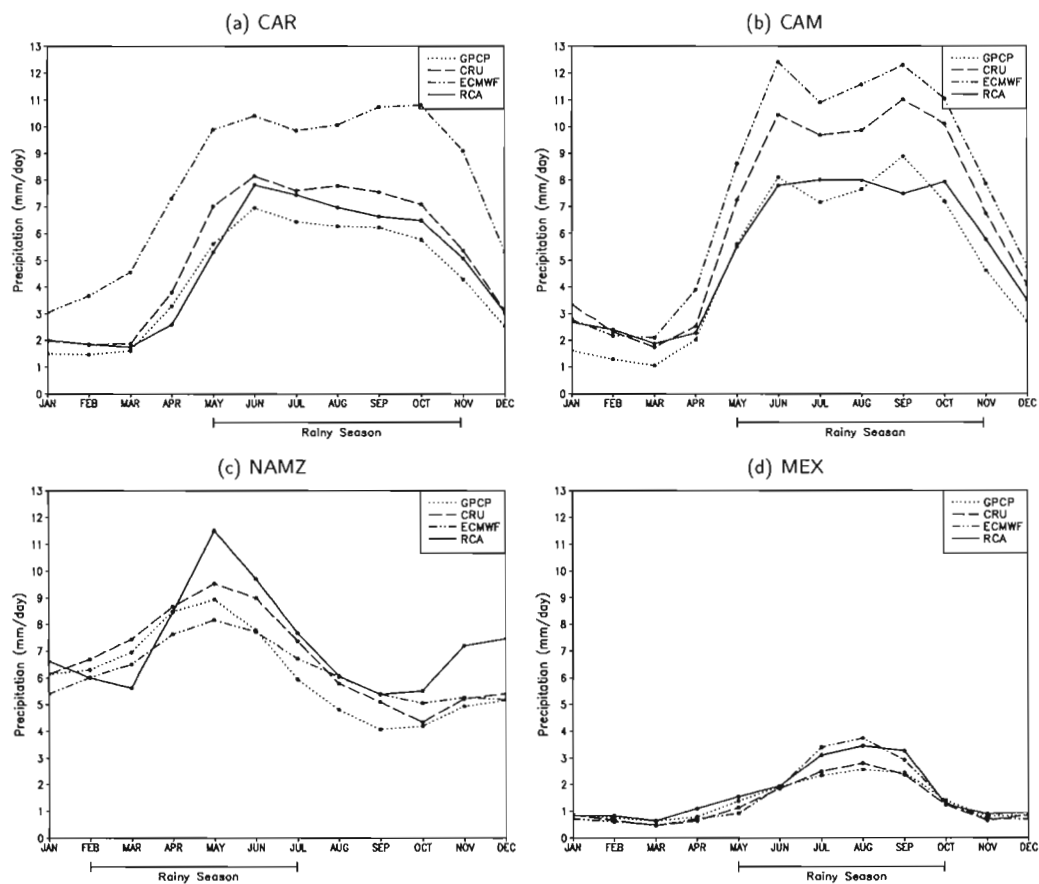
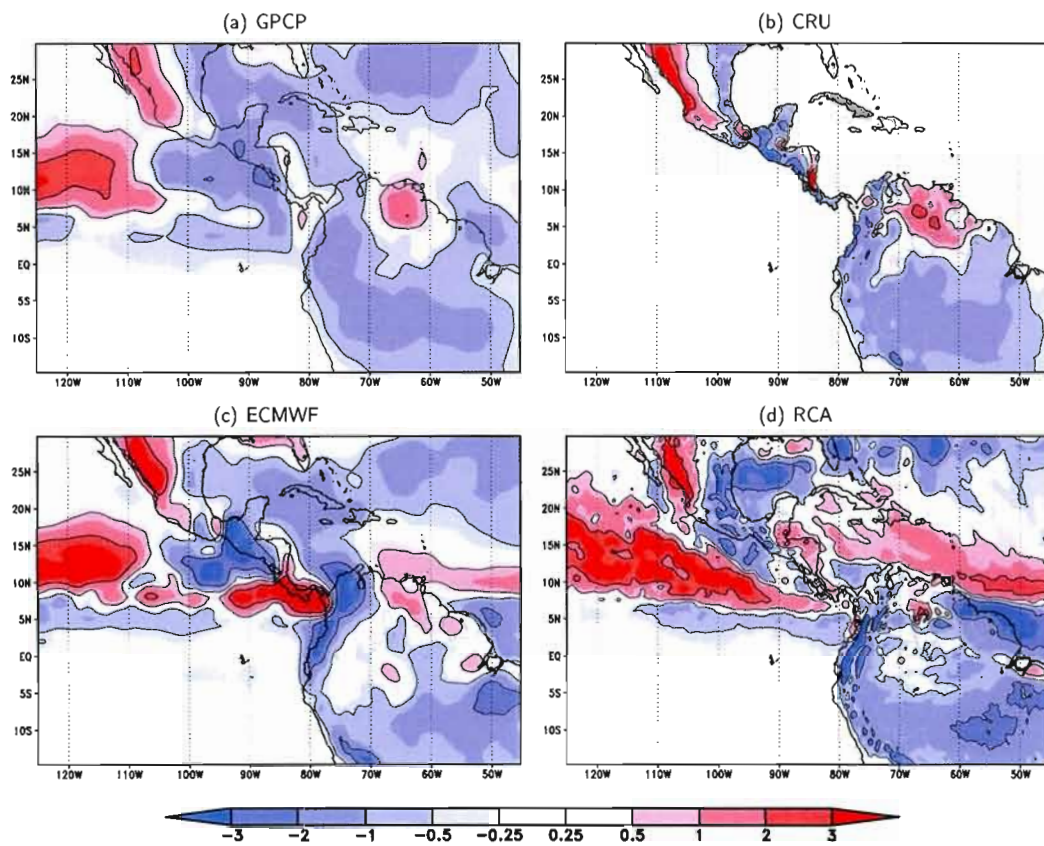


Figure 1.3 Climatological precipitation (mm/day) / seasons JFM and JAS (columns) / GPCP, CRU, ECMWF and RCA (rows).



**Figure 1.4** Spatial mean climatological precipitation over land, annual cycle by region. The duration of the climatological rainy season is indicated for each region on the x-axis.



**Figure 1.5** Climatological average of July and August minus the average of June and September precipitation (mm/day).

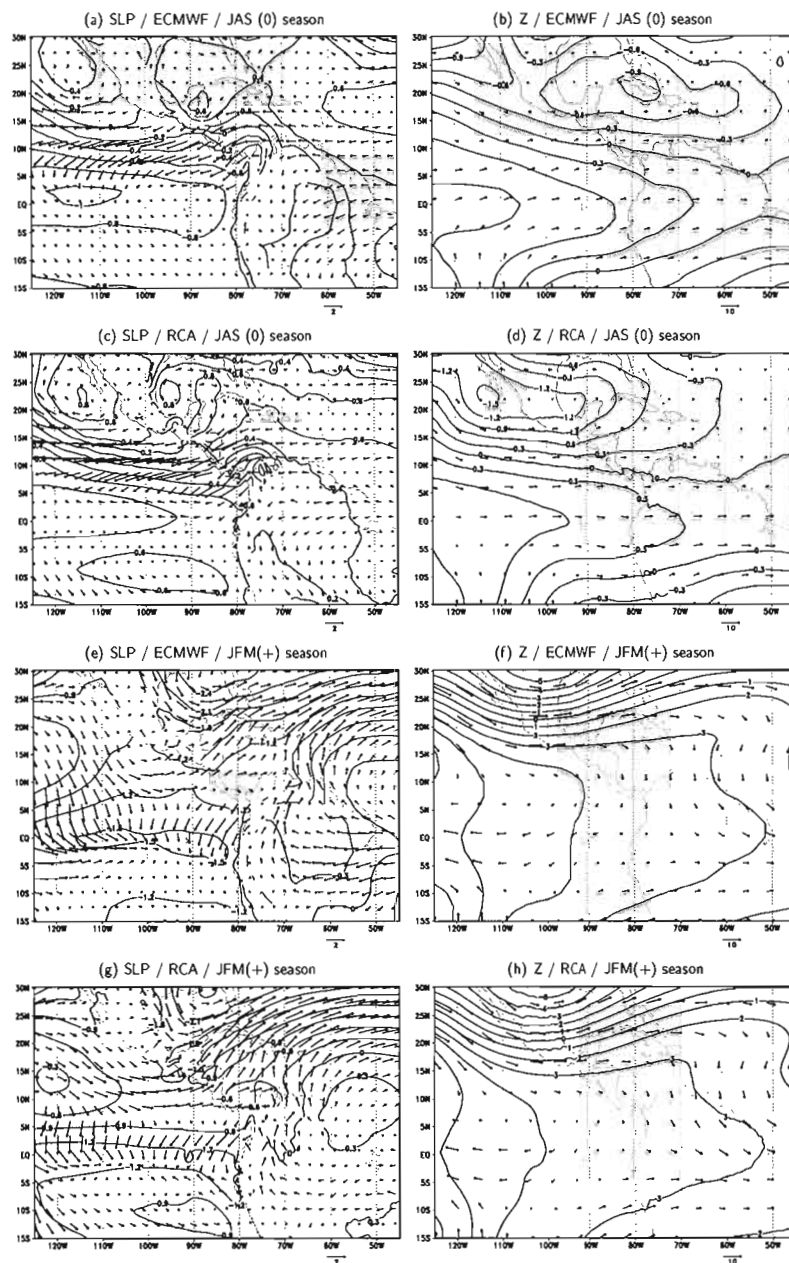


**Figure 1.6** El Niño anomalies (*NINOA*) of : SLP (contours in hPa) and 925 hPa winds (vectors in m/s) in left column, 250 hPa geopotential height (contours in dam) and winds (vectors in m/s) in right column. Full lines indicate positive anomalies and dotted lines indicate negative anomalies. The scale of the wind vectors is indicated on each figure.

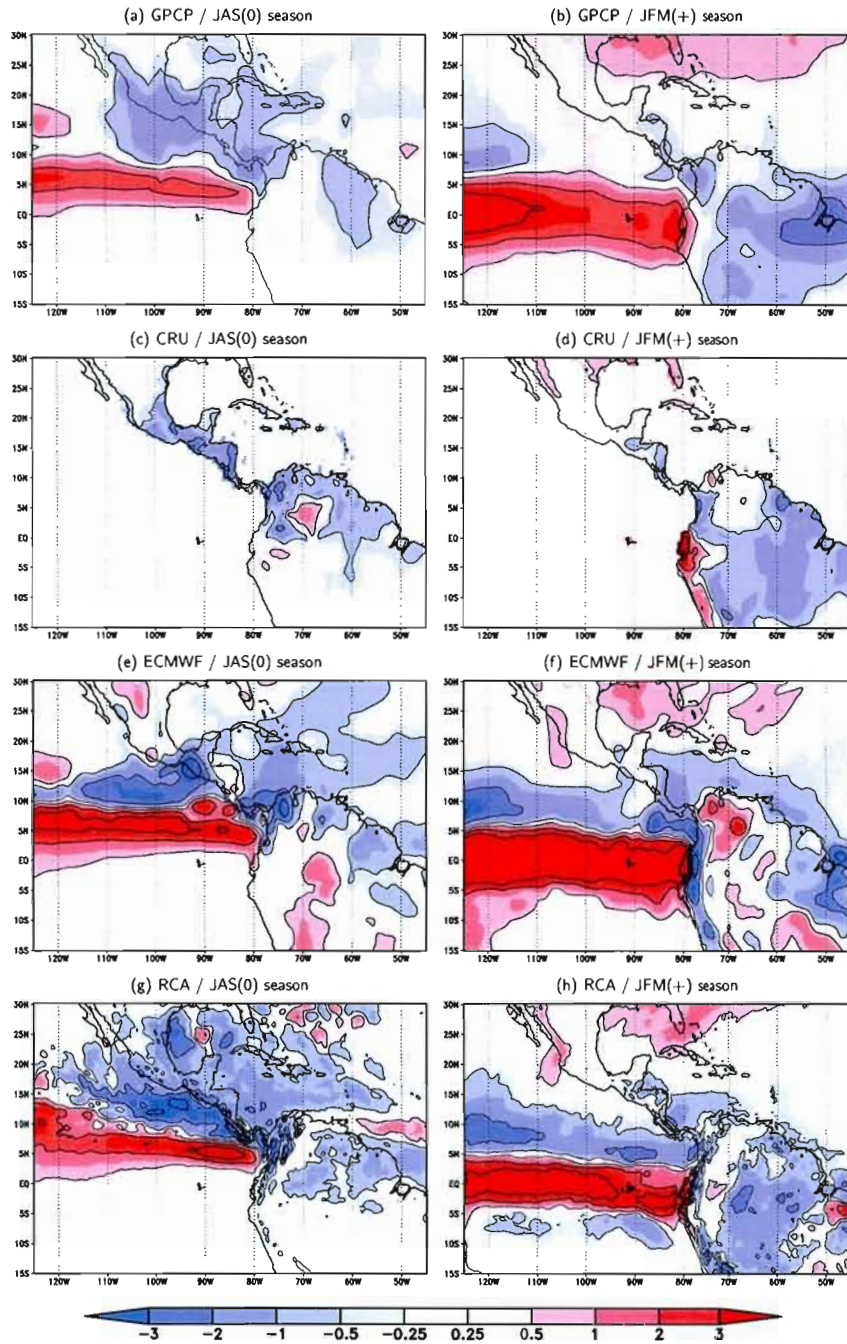


**Figure 1.7** El Niño anomalies (*NINOA*) of precipitation (mm/day) / seasons JAS(0) and JFM(+) (columns) / GPCP, CRU, ECMWF and RCA (rows).

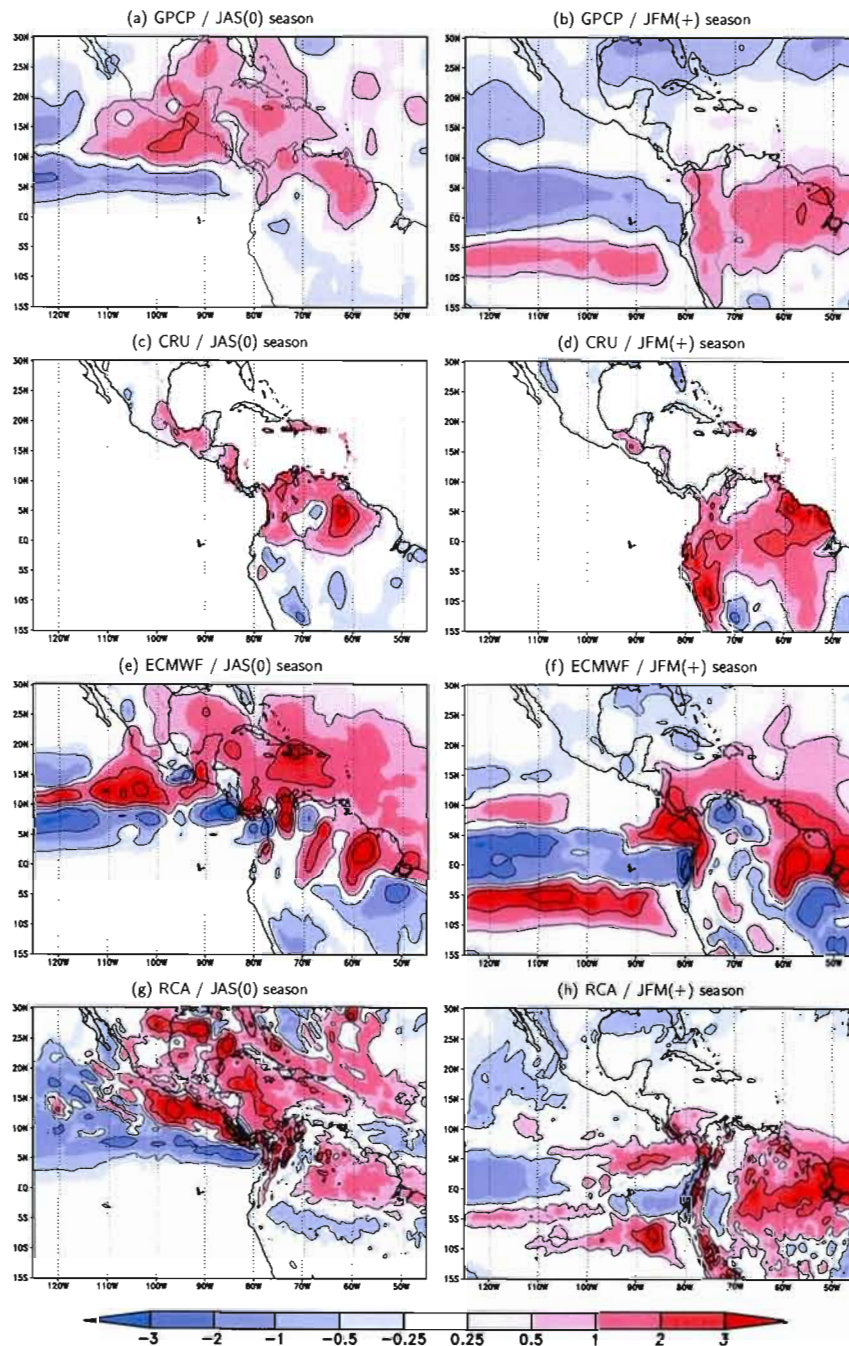
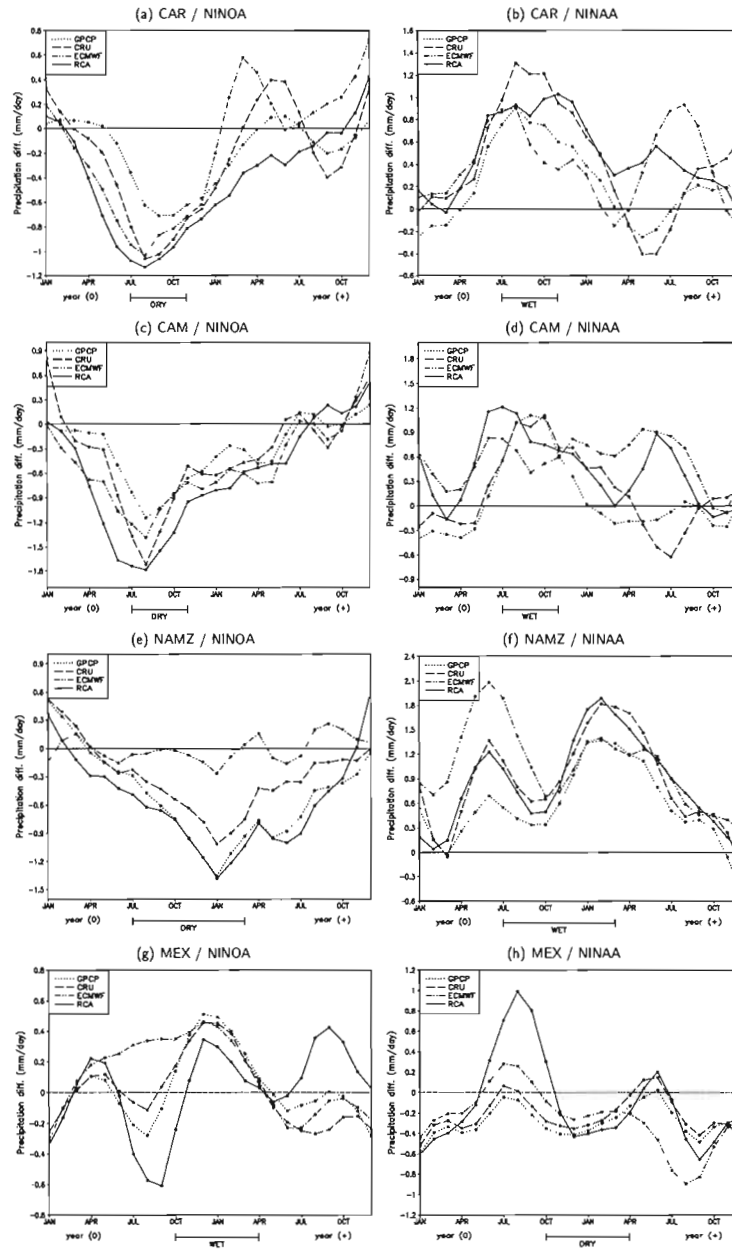
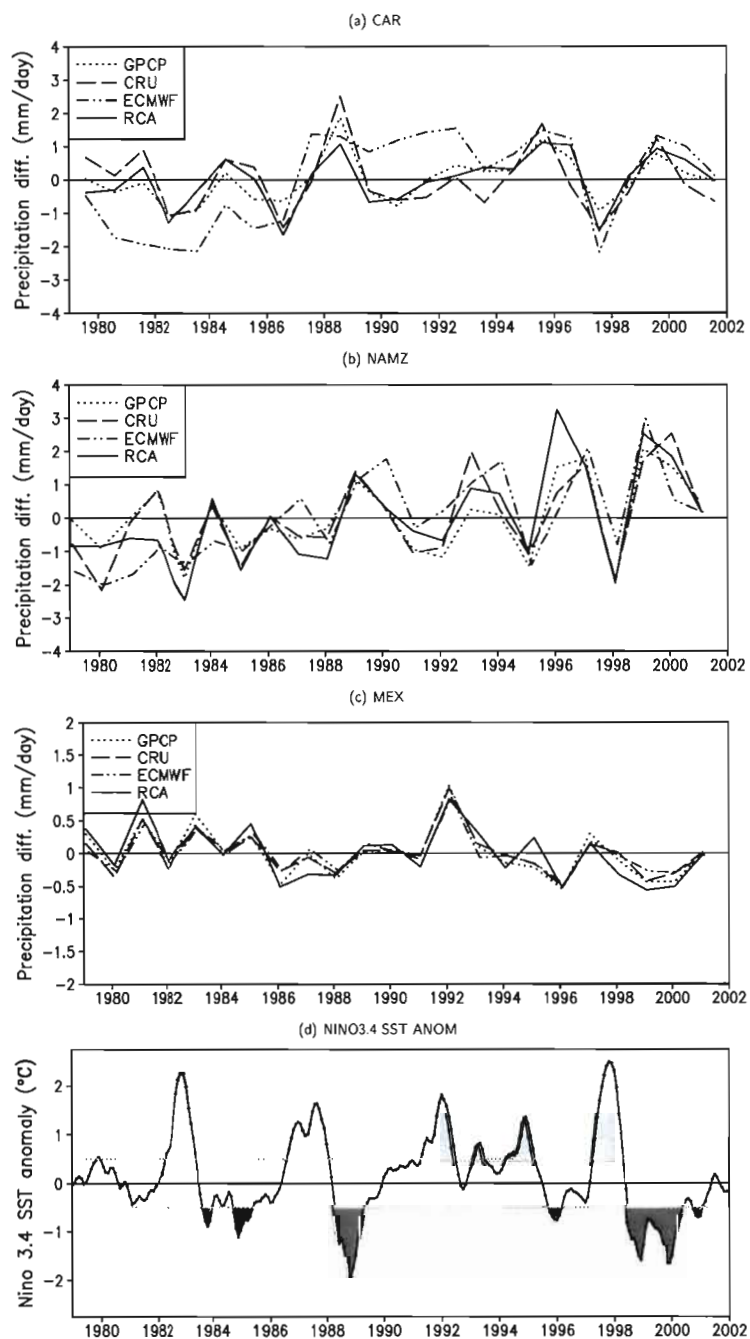


Figure 1.8 As Figure 1.7 but La Niña anomalies (*NINAA*) of precipitation (mm/day).



**Figure 1.9** El Niño (left column) and La Niña (right column) anomalies of precipitation (mm/day) over land, annual cycle by region. The typical period and impact (wet/dry) of ENSO variability for each region is indicated on the x-axis. The scales on the y-axis are different in each plot.



**Figure 1.10** Time series of precipitation anomalies over land (mm/day) / regions (a) CAR(season JAS) (b) NAMZ(season JFM) and (c) MEX(season JFM); (d) Niño 3.4 SST anomaly ( $^{\circ}\text{C}$ ).

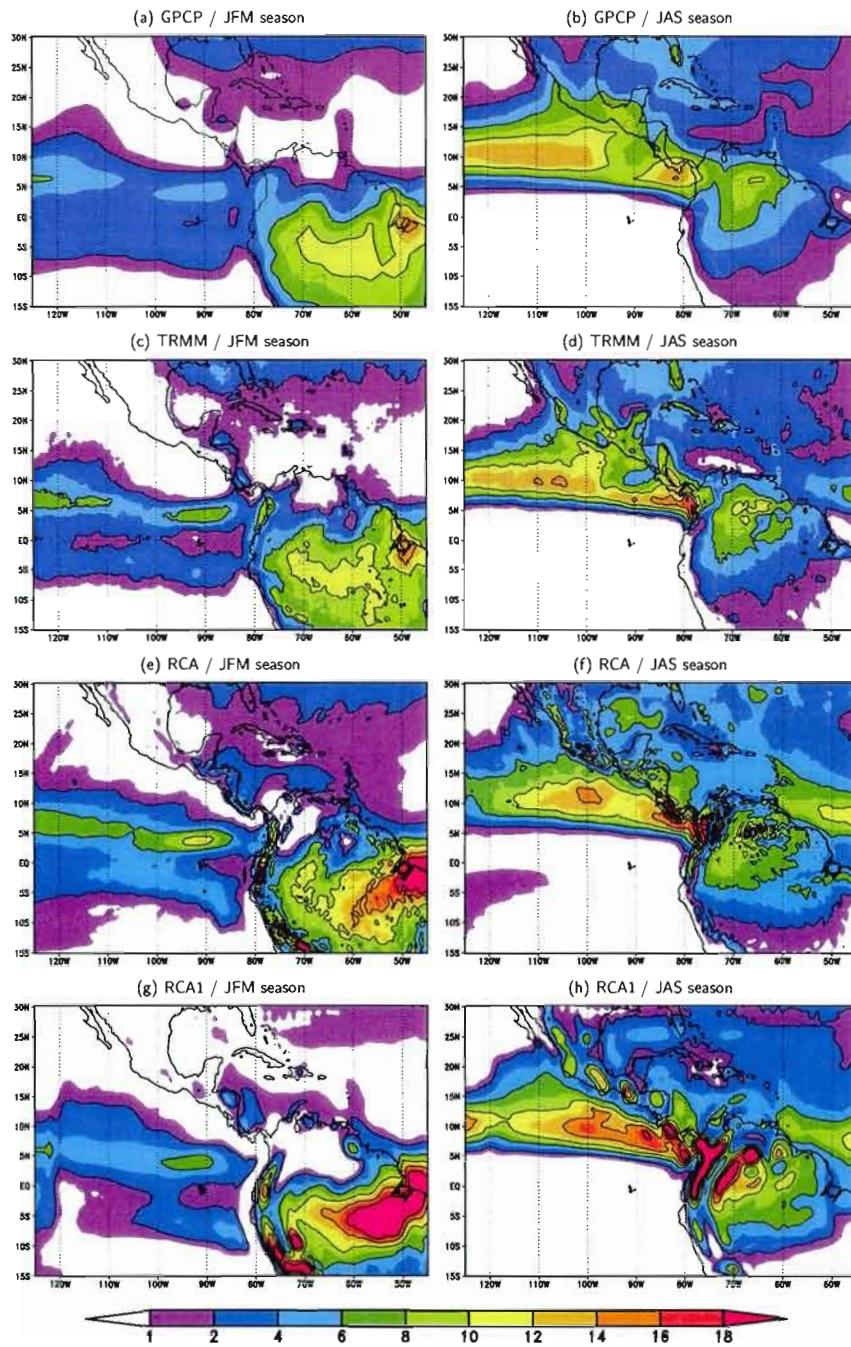


**Figure 1.11** Climatological precipitation (mm/day) during the 1998-2005 period / seasons JFM and JAS (columns) / GPCP, TRMM, RCA and RCA1 (rows).

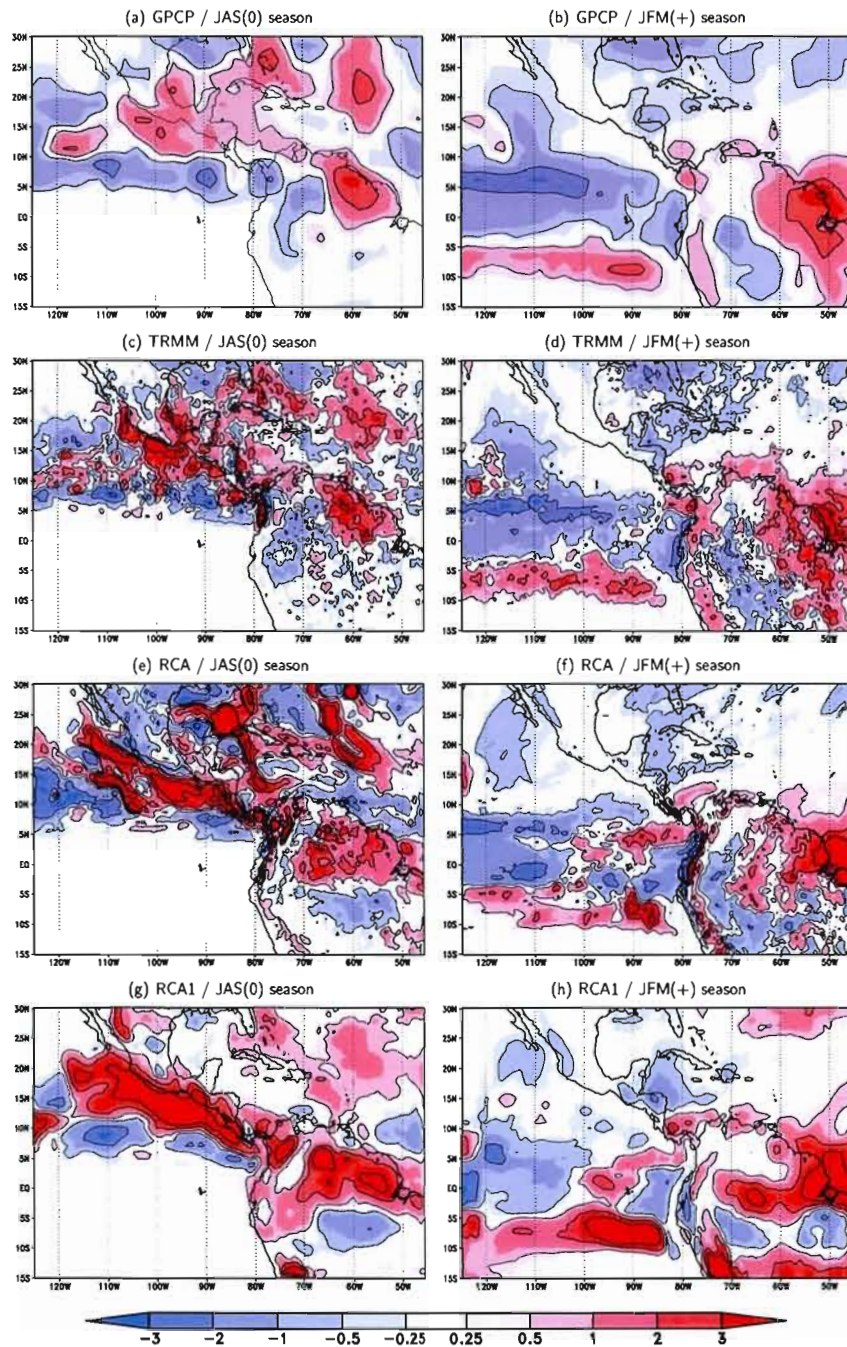


**Figure 1.12** Precipitation anomaly (mm/day) during the 1999-2000 La Niña / seasons JAS(0) and JFM(+) (columns) / GPCP, TRMM, RCA and RCA1 (rows).

**Table 1.1** Strong ENSO events in the 1979-2005 period

El Niño	La Niña
1982-1983	
1986-1987	1988-1989
1991-1992	
1997-1998	1998-1999
2002-2003	1999-2000

**Table 1.2** Linear correlation (RCA vs. observations and ECMWF vs. observations) of seasonal anomalies of precipitation over land. Bold values are significant at 99% level, others at 95% level (except those in parentheses).

Region	Obs.	RCA		ECMWF	
		All	ENSO	All	ENSO
CAM	GPCP	0.51	(0.75)	0.50	(0.64)
	CRU	<b>0.65</b>	0.84	<b>0.66</b>	0.82
CAR	GPCP	<b>0.84</b>	<b>0.90</b>	<b>0.68</b>	0.83
	CRU	<b>0.76</b>	<b>0.92</b>	(0.37)	0.76
MEX	GPCP	<b>0.90</b>	<b>0.97</b>	<b>0.96</b>	<b>0.99</b>
	CRU	<b>0.88</b>	<b>0.97</b>	<b>0.97</b>	<b>0.99</b>
NAMZ	GPCP	<b>0.88</b>	<b>0.98</b>	<b>0.64</b>	0.86
	CRU	<b>0.82</b>	<b>0.96</b>	<b>0.70</b>	(0.73)

## CHAPITRE II

### ARTICLE II : ÉCHELLE INTRASAISSONNIÈRE

**An Analysis of Regional Climate Model Performance Over the Tropical Americas. Part II : Simulating Subseasonal Variability of Precipitation Associated with ENSO Forcing**

Etienne Tourigny

Université du Québec à Montréal, Montréal, Canada

Colin G. Jones

Université du Québec à Montréal, Montréal, Canada

Submitted to Tellus (April 3, 2008)

First revision (October 2, 2008)

## ABSTRACT

The El Niño/Southern Oscillation (ENSO) constitutes a major source of potential predictability in the tropics. The majority of past seasonal prediction studies have concentrated on precipitation anomalies at the seasonal mean timescale. However, fields such as agriculture and water resource management require higher time frequency forecasts of precipitation variability. Regional Climate Models (RCMs), with their increased resolution, may offer one means of improving General Circulation Model (GCM) forecasts of higher time frequency precipitation variability.

Part I of this study evaluated the ability of the Rossby Center Regional Atmospheric Model (RCA), forced by analysed boundary conditions, to simulate seasonal mean precipitation anomalies over the tropical Americas associated with ENSO variability. In this paper the same integrations are analyzed, with the focus now on precipitation anomalies at subseasonal (pentad) timescales.

RCA simulates the climatological annual cycle of pentad-mean precipitation intensity quite accurately. The timing of the rainy season (onset, demise and length) is well simulated, with biases generally of less than two weeks. Changes in the timing and duration of the rainy season, associated with ENSO forcing, are also well captured. Finally, pentad-mean rainfall intensity distributions are simulated quite accurately, as are shifts in these distributions associated with ENSO forcing.

## 2.1 Introduction

Regional Climate Models (RCMs) are increasingly being used in tropical regions to downscale Global Climate Model (GCM) simulations of seasonal and interannual variability (Sun et al., 2006; Seth et al., 2007, and references therein). The increased resolution of RCMs, compared to GCMs, allows for a potentially more accurate simulation of regional climatic features, particularly those resulting from localized surface forcing or organized on small scales. Moreover, statistical or dynamical downscaling of GCM forecasts may improve the simulation of important meteorological variables at high time frequency (Goddard et al., 2001). The coupled ocean-atmosphere phenomenon known as the El Niño/Southern Oscillation (ENSO) is the leading mode of interannual Sea Surface Temperature (SST) variability in the tropics (Wang et al., 1999). It follows that RCMs when forced by ENSO-related SST and large-scale atmospheric forcing should show some skill in simulating seasonal and subseasonal precipitation anomalies in the tropics. In this work we will analyze the ability of a RCM to represent subseasonal regional scale anomalies over Central and South America, occurring under El Niño and La Niña conditions, when the RCM is forced by observed SSTs and analysed lateral boundary conditions. As discussed in a companion paper (Tourigny et Jones, 2008a), hereafter referred to as TJ2008a, this exercise should be viewed as a necessary first evaluation step, before the RCM is forced by boundary conditions derived from a free-running GCM.

El Niño conditions are associated with anomalous warm waters in the equatorial central and east Pacific. This leads to an increase in deep convection in those regions and anomalous rainfall in other regions of the globe through various atmospheric and oceanic teleconnections (Alexander et al., 2002). La Niña conditions show largely converse behavior, with cold SST anomalies and a reduction in convective activity in the equatorial central and east Pacific. The SST and convection anomalies force identifiable seasonal mean precipitation anomalies over the tropical Americas. In TJ2008a we assessed the ability of a RCM to downscale the large scale signature of these anomalies at the sea-

sonal mean timescale. In this paper we extend this analysis to higher time frequency anomalies in precipitation over the tropical Americas. As in similar studies (Ropelewski et Halpert, 1987, 1996) we define composite years (0), and (+), which represent the years during and after “typical” ENSO events, with the peak of anomalous SST in the OND(0) season (i.e. October-December of year (0)).

A number of studies have identified interannual variability of the rainy season onset and demise over the tropical Americas associated with ENSO forcing. Enfield et Alfaro (1999) showed that over Central America the rainy season onset is correlated with North Atlantic SSTs and that the demise of the rainy season is correlated with both North Atlantic and ENSO-related (east Pacific) SST variability. A warm east Pacific (El Niño conditions) is associated with an early demise of the rainy season in year (0) over Central America, consistent with dry conditions observed from July-October (0) (whereas La Niña conditions cause a late demise of the rainy season). As the rainy season over Central America extends from May-October and the ENSO-related anomalies are from July-October (0), it is clearly only the demise of the rainy season that is likely to be affected by ENSO variability.

El Niño conditions reduce Sea Level Pressure (SLP) in the northern tropical Atlantic in winter (+), weakening the easterly trade winds and causing a reduction in moisture convergence into the Amazon basin (Nobre et Shukla, 1996). This leads to decreased convection (Marengo, 1992; Marengo et Hastenrath, 1993) and a delay in the onset of the rainy season (and to a lesser extent an early demise) (Liebmann et Marengo, 2001; Marengo et al., 2001) in the northern Amazon, while the converse is generally true for La Niña conditions. There is also evidence of tropical Atlantic SST variability, independent of ENSO forcing, influencing moisture transport into the Amazon (Fu et al., 2001, and references therein). Moreover, Liebmann et Marengo (2001) found that SST anomalies influence the timing of the rainy season but not the intensity of precipitation within the rainy season over the Amazon.

Regarding ENSO impacts on the intensity distribution of higher time frequency preci-

precipitation, Seth et al. (2004) have shown distinct changes in the intensity distribution of daily precipitation over the Amazon basin, between one El Niño year (1983) and a single La Niña year (1985). Specifically they found, for the period January-May (+), a shift in the distribution resulting in more frequent weak precipitation events and a reduction in the number of intense events. Rauscher et al. (2007) also found a shift towards more weak rainfall events during El Niño years and a converse shift towards more intense rainfall events during La Niña years over northeast Brazil. These two studies show that a dry seasonal anomaly comes about mainly from a reduction in the number of days with moderate to intense precipitation and an increase in the number of days with weak or no rainfall. The RCM used in these two studies (RegCM3) generally succeeded in simulating these intensity distribution changes.

In this work we use the Rossby Center Regional Atmospheric Model version 3 (referred to as RCA) (Jones et al., 2004; Kjellström et al., 2005) to study the simulated variability of subseasonal precipitation over Central and South America, associated with ENSO-related variability. Part I of this study (TJ2008a) looked at regional-scale variability of precipitation associated with ENSO at seasonal mean timescales. We found that RCA was able to reproduce most of the seasonal climatological features of precipitation over the domain of study, as well as capturing the main observed anomalies related to ENSO SST forcing. Here observed pentad-mean values of precipitation are used in order to evaluate the ability of RCA to simulate both the climatology and ENSO-related variability of pentad timescale precipitation using the following metrics : 1) the annual cycle of pentad-mean precipitation ; 2) rainy season onset, demise and duration and 3) subseasonal (pentad) intensity distributions. Details of the various diagnostics metrics used in the model evaluation appear in both section 2.2.2 and at the relevant results sections of the article.

## 2.2 Model Configuration and Analysis Methods

For details on model setup, experimental procedure and domain of analysis the reader is referred to TJ2008a. The regions analyzed, shown in Figure 1 of TJ2008a, are : MEX (northern Mexico), CAR (Caribbean), CAM (Central America) and NAMZ (northern Amazon).

### 2.2.1 Observations

A study of precipitation anomalies at subseasonal timescales should ideally use daily or even sub-daily precipitation observations. Reliable daily observations are scarce in Central America and the Caribbean, and gridded products are non-existent. South America on the contrary has a denser observation network and a few gridded products are available. This study uses the “Daily Precipitation Grids for South America” from Liebmann et Allured (2005) (hereby referred to as LASA). The current version (SA19) is available at a resolution of  $1^\circ$  over land points with temporal coverage from January 1940 to August 2006. Liebmann and Allured have also prepared a similar dataset (NA1) which covers the United States and parts of Mexico, with temporal coverage from January 1940 to December 2004. This dataset is used over the MEX region of our domain and is referred to as LANA. Reanalysis products, such as the ERA-40 reanalysis (Uppala et al., 2005) from the European Centre for Medium-Range Weather Forecasts (ECMWF) and the NCEP/NCAR Reanalysis, offer sub-daily precipitation estimates. These products, however, suffer from deficiencies in the tropics (such as an over-estimate of rainfall intensity) which limit their use as an observational surrogate. To illustrate this we combine the ERA-40 reanalysis and ECMWF operational analysis daily data (from August 2002) into one dataset which we name ECMWF and use as a point of reference. A recent study by Ropelewski et Bell (2008) suggests that the gridded LASA dataset is more suitable than reanalysis data (or even station data) for a study such as ours evaluating simulated shifts in daily rainfall over South America associated with ENSO.

The scarcity of gridded daily observations over Central America and the Caribbean has

forced us to turn to satellite-based pentad observations. We chose the GPCP Pentad Precipitation (hereby referred to as GPCP), described by Xie et al. (2003). The GPCP pentad data is at a relatively low resolution ( $2.5^\circ$ ), but covers a long time period (1979-present) allowing an evaluation of numerous ENSO events, hence it is used as the main observational dataset in this study. Higher temporal and spatial resolution observations, such as the Tropical Rainfall Measuring Mission (TRMM) 3B42 product (Huffman et al., 2007) and GPCP 1DD (Huffman et al., 2001), respectively at  $0.25^\circ$  and  $1^\circ$  spatial resolution and three hourly and daily temporal resolution, would be better suited for RCM evaluation of subseasonal precipitation. Unfortunately these datasets are limited in temporal extent, available from 1998 and 1997 respectively and therefore do not allow an extensive evaluation of simulated ENSO variability. We nevertheless use the TRMM 3B42 dataset for the 1998-2004 period and compare it to GPCP and RCA, as well as a lower-resolution ( $1^\circ$ ) version of the RCA model (RCA1). This allows us to evaluate the potential added value of using a high resolution RCM with respect to small scale precipitation variability and also to assess the reliability of the low-resolution GPCP dataset.

### 2.2.2 Methods

Our main emphasis is on the 1979-2004 period, during which the model is compared to GPCP and ECMWF in all regions, the LASA dataset is also used over the NAMZ region, while LANA provides an additional observational constraint over the MEX region. Daily precipitation values are averaged at the pentad (5 day) timescale. In an effort to limit discrepancies due to differing resolutions, all observations and the model output are interpolated to a uniform  $1^\circ \times 1^\circ$  grid using bilinear interpolation. The method used to define the warm and cold ENSO events is based on SST anomalies over the Niño 3.4 region and is outlined in section 4.2 of TJ2008a. We choose only the strongest ENSO events (shown in Table 1 of TJ2008a) in order to obtain a clear anomaly signal.

Three diagnostic methods are used to assess the ability of RCA to simulate pentad

timescale precipitation. First we analyse the climatological annual cycle of pentad mean precipitation for the four regions of interest. We also study composites of El Niño and La Niña anomalous pentad mean precipitation as a function of the annual cycle. Secondly we evaluate the model’s ability to simulate the timing of the onset and demise of the rainy season in each region and any variability of these quantities associated with ENSO forcing. Third we analyse the simulated pentad-mean precipitation intensity distribution for each region, during their respective rainy seasons, and spatially over the entire model domain. We evaluate both the climatological intensity distribution and shifts in this distribution during ENSO years.

For the spatially averaged climatologies and the ENSO-related anomalies, grid box values of each of the variables are spatially averaged over each of the regions of interest for every year. We first calculate the climatological average of a given variable over all years (1979-2004). In order to evaluate the interannual variability associated with ENSO forcing, we calculate ENSO composites which are the average of El Niño or La Niña years separately, considering years (0) and (+) of the ENSO events, as the atmospheric responses show a temporal evolution during a “typical” ENSO event of two years. The ENSO signal is easier to evaluate when the composites are given as anomalies or differences from climatology. The resulting metrics are thus defined as :

$$NINOA = \overline{NINO} - CLIM \quad (2.1)$$

$$NINAA = \overline{NINA} - CLIM \quad (2.2)$$

where  $\overline{NINO}$  and  $\overline{NINA}$  are the basic ENSO composite values of a given variable,  $CLIM$  is the climatological average of the same variable and  $NINOA$  and  $NINAA$  are the anomalies of the ENSO composites, with all values being at the pentad timescale.

## 2.3 Results

### 2.3.1 Annual Cycle of Precipitation

This section discusses the annual cycle of pentad-mean precipitation, with results from RCA, GPCP and ECMWF. Figure 2.1a-d shows the climatological average for all years of the study (1979-2004) for all four regions. On the x-axis of the climatological precipitation figures we indicate the typical rainy season duration (rounded to the beginning of the month), as derived from the GPCP data in Table 2.1 which details the observed, climatological onset and demise dates of the rainy season by region. Details on the method for calculating these dates are given in section 2.3.2. Figure 2.1e-f gives the anomalous precipitation for the El Niño (*NINOA*) composites, expressed as absolute deviations from the climatology in mm/day, for regions CAR and NAMZ only. These regions contain the main anomalies associated with ENSO, for details concerning the other regions refer to the seasonal mean anomalies outlined in TJ2008a. On the x-axis we indicate the generally accepted time periods, within the annual cycle, of El Niño forced precipitation anomalies (dry/wet) with respect to each region (Ropelewski et al., 1987, 1989, 1996). This is done to highlight when and where ENSO forced anomalies impact on the climatological rainy season. Similar results are given for all regions and both El Niño and La Niña composites in TJ2008a at monthly timescales.

The CAR region (Figure 2.1a) has a distinctive rainy season from May-October (inclusive), which RCA captures quite accurately, with a wet bias of  $\approx 1$  mm/day throughout the rainy season and slight dry bias at the beginning. ECMWF shows a large wet bias over the Caribbean and Central America. In the CAM region (Figure 2.1b) the model performance is quite accurate, except for a poor representation of the Mid-Summer Drought (MSD) (Small et al., 2007). The MSD is recognized as a drop in precipitation in July-August, followed by a second maximum peak in precipitation in September. RCA does show a slight drop in July, but fails to recover in September, exhibiting a dry bias. In TJ2008a we showed that the basic dynamical and precipitation features

of the MSD were simulated by RCA, but due to an incorrect spatial distribution and intensity of localized precipitation maxima and minima (mostly over the western Caribbean), the MSD doesn't appear in the simulated spatial averages over CAM at monthly timescales. Close inspection of pentad-mean values shows that the MSD is present in the RCA results, although with reduced amplitude compared to observations.

Over the NAMZ region (Figure 2.1c) the rainy season is from February-June. While RCA correctly simulates the beginning of the rainy season, there is a clear wet bias starting in May and extending through the year. RCA also exhibits a second maximum in precipitation in November-December, a problem common to many climate models in the Amazon; related to semi-annual solar forcing (Rauscher et al., 2007; Seth et al., 2007). The overall intensity of ECMWF precipitation is more comparable to the observations over NAMZ, although the amplitude of the annual cycle is too weak.

The MEX region (Figure 2.1d) has a drier climate, with a weak rainy season from May-September. The model climatology agrees well with observations, except for a small wet bias ( $\sim 1$  mm/day) during the rainy season, similar to ECMWF. The wintertime wet anomaly (for *NINOA*) and dry anomaly (for *NINAA*) over MEX are seen both in the model and observations (not shown, see TJ2008a for an example of seasonal mean anomalies). In this region the main periods of ENSO forcing fall outside the rainy season and therefore have only a minimal impact on simulated rainfall statistics.

We discuss here the pentad-timescale El Niño anomalies shown in Figure 2.1e-f. In the CAR region, the anomalous dry period of July-October (0), associated with ENSO forcing, is generally well simulated by RCA although with slightly weaker variability than seen in the observations. RCA clearly shows a stronger and more constant dry anomaly than observed over CAR in the period May-July (0). This translates into a seasonal mean dry bias, possibly due to RCA being excessively sensitive to anomalous subsidence (for further details refer to TJ2008a). From spring (+) onward there is limited predictability associated with ENSO, as a result there is only limited correspondence in the time evolution of the simulated and observed anomalies. It is noteworthy that

RCA values generally follow more closely the GPCP observed anomalies than does the ECMWF analysed data.

Over NAMZ the documented ENSO-related dry period of July (0)-March (+) is well simulated by RCA (Figure 2.1f). Similar but opposite signed anomalies in La Niña are also captured by the model (see TJ2008a for La Niña seasonal mean anomalies). The maximum observed negative anomalies are in January, the month prior to the onset of the rainy season, suggesting an important ENSO-related impact on the rainy season onset. During the rainy season the observed anomalies are smaller, of the order of  $\approx 1-2$  mm/day. RCA generally captures the observed high frequency variability of precipitation, in particular the large positive and negative anomalies between January (+) and July (+). This indicates the ability of a RCM to simulate subseasonal precipitation variability on the regional scale when forced by realistic large scale atmospheric variability and SST anomalies.

### 2.3.2 Rainy Season Onset, Demise and Duration

The prediction of the timing of the rainy season (onset and demise) is strongly linked to the prediction of total rainfall accumulation during the rainy season and is important in fields such as agriculture (Marengo et al., 2001). From a societal impact perspective, an accurate prediction of changes in the onset and/or demise of the rainy season may in fact be more important than an accurate prediction of seasonal mean precipitation anomalies. In this study the rainy season onset and demise dates are calculated using the “Anomalous Accumulation” method of Liebmann et Marengo (2001) using pentad mean data rather than daily data. We chose this method because it does not use a regionally-defined (arbitrary) threshold of precipitation intensity [such as e.g. Higgins et al. (1999) and Marengo et al. (2001)], and therefore should be applicable to different regions that exhibit different rainy season characteristics. The anomalous accumulation  $A$  is defined at each grid point and each pentad as :

$$A(p) = \sum_{n=p0}^p (R(n) - \bar{R}) \quad (2.3)$$

where  $R(n)$  is the pentad mean precipitation for pentad  $n$  and  $\bar{R}$  is the climatological mean pentad averaged over the entire period of the study.

For each grid point and each year we start the calculation two months after the end of the climatological rainy season for that grid point, to account for interannual fluctuations in the demise of the rainy season. The onset and demise of each rainy season are defined respectively as the minimum and maximum of  $A$  for each year of calculation. For each region and year an average is calculated over all the grid points of the particular region.

The climatological onset and demise dates for each region, along with average dates for the El Niño and La Niña composites, are listed in Table 2.1. The results for individual years are shown in Figure 2.2, where the relevant El Niño and La Niña years are indicated by large grey and black tick marks along the x-axis. It should be noted that, for the regions CAR and CAM, the ENSO composites are computed for the years (0), whereas for the NAMZ and MEX regions, the years (+) are used to isolate the years in the ENSO cycle where ENSO impacts are felt in each respective region. For example, in the NAMZ region the important ENSO anomalies are before the rainy season of year (+), therefore we compute the timing of the rainy season during the years (+) of the ENSO events.

Average results for the CAR region (Table 2.1) show that onset occurs during the month of May and RCA tends to show a later onset of two pentads compared to GPCP. The average demise is at the beginning of November and is well simulated. Onset and demise are shifted two weeks early in ECMWF (compared to GPCP) both on average and for individual years. The observed onset of the rainy season in years (0) is later in El Niño years and earlier in La Niña years over CAR, while RCA captures this general trend it exhibits more variability than seen in GPCP. The demise of the rainy season over CAR shows strong variability related to ENSO ( $\approx 15$  days early in El Niño and  $\approx 15$  days late

in La Niña) for both model and observations. In Figure 2.2a the 1997 El Niño shows a shorter rainy season most apparent in the extreme early demise ( $\approx$ one month early), which is well captured by RCA. All La Niña events (1988, 1998 and 1999) show a late demise of the rainy season over CAR, which is also generally well simulated. Values for CAM are largely similar, except that the rainy season starts 3 pentads later on average and the ENSO-related variability is smaller. The presence of the Mid-Summer Drought (discussed in section 2.3.1) in the CAM region, which can be seen as a series of two rainy seasons, can be challenging for the “anomalous accumulation” method. Close inspection of time series has shown that the technique is adequate under most circumstances, but shows a much too early rainy season demise (by a few weeks) in the extreme case of the 1986 El Niño, while other anomalous years (such as the 1997 El Niño) are correctly calculated.

For the NAMZ region (Table 2.1), rainy season onset occurs on average at the end of January, with the simulated onset in RCA delayed by 1-2 pentads. The demise occurs in July and RCA shows a significantly late average date, while the length of the rainy season is well simulated; the same general conclusions also hold for ECMWF. The late onset and demise in RCA (most evident when compared to LASA) are due to deficiencies in the simulated annual cycle (Figure 2.1c). The late onset in RCA over NAMZ is likely a result of the secondary (incorrect) precipitation maximum in December, leading to decreasing precipitation rates throughout January. This causes the variable  $A(p)$  to continue to decrease through January and into February. In the observations, the smaller precipitation in December-January leads to the minimum in  $A(p)$  being found earlier in the year. With respect to the late decay in RCA, we believe this is related to the excessive precipitation in the model during the period April-July. This leads to the variable  $A(p)$  continuing to increase through June and July, whereas the lower observed rainfall rate in this period leads to  $A(p)$  reaching a maximum a few weeks earlier in the observations.

GPCP and LASA show sensitivity to ENSO forcing in the onset and demise of the rainy

season of year (+) over NAMZ (late onset, early demise and shorter rainy season during El Niño events and the converse for La Niña events). The model generally captures this variability quite accurately, while ECMWF only shows changes in the La Niña events. The highest observed and modeled sensitivity to ENSO forcing is seen in an early onset during La Niña events (e.g. 1989 and 1999 where the onset is  $\approx$ one month early). Over NAMZ there are some years that show a change in the rainy season onset and/or demise which are not associated with ENSO forcing, in both model and observations (e.g. 1996). This is likely related to changes in Atlantic SSTs, independent of ENSO variability, which have a coherent impact on moisture convergence and rainy season onset over NAMZ. As RCA uses observed SSTs and analysed LBCs any coherent forcing from Atlantic SST anomalies will likely be available to the model. It is noteworthy that ECMWF analysed precipitation does not show an early onset in 1996 in disagreement with both observation datasets.

In the MEX region (Table 2.1) rainy season onset occurs at the beginning of May. RCA shows a slightly earlier onset on average compared to observations. The demise occurs on average at the beginning of October for the observations, but four pentads earlier for RCA. This is consistent with the annual cycle results (see Figure 2.1d), where a sharp drop in the simulated precipitation is seen in mid-September. The biases in onset and demise (also seen in Figure 2.2d) exhibit significant year-to-year variability and result in a shorter rainy season for RCA and ECMWF on average. Although the match between model and observations in this region is the weakest, RCA does capture some of the ENSO-related variability in the timing of the rainy season. As the main ENSO forced precipitation anomalies occur during the winter season, hence outside of the rainy season, we would expect less predictability in the changes in the timing of the rainy season. There is however a general tendency towards early onset/late demise in the rainy season of years (+) of the El Niño composites, and the converse for La Niña years, which is well captured by the model.

### 2.3.3 Intensity distribution of precipitation

An accurate prediction of precipitation intensity distribution is important in fields such as water management and agriculture (Seth et al., 2004), where the distribution of rainfall intensity is at least as important as the seasonal mean value.

#### 2.3.3.1 Histograms by Region

Pentad-mean intensity distributions are evaluated during the rainy season of each of the four regions. As was shown earlier, there is considerable interannual variability in the onset, demise and length of the rainy season in each region. Much (but not all) of this variability is associated with ENSO forcing. Our goal is to evaluate the changes in the intensity distribution *during* the rainy season associated with ENSO forcing, independent from the changes in the timing of the rainy season. In order to do this, for each individual year and each region we compute precipitation intensity distributions within the onset and demise dates of the rainy season for that particular year (the calculation of which follows the method described in the previous section). This is done for model and observations separately. In doing so we evaluate if the shifts in the distribution are primarily attributable to changes *within* the rainy season of each year or rather to changes in the *duration* of the rainy season.

Figure 2.3 shows the area-averaged, precipitation intensity distribution binned into six categories for each of the four regions, averaged over each of the (variable-length) rainy seasons. The first three bins (0-1, 1-2.5 and 2.5-5 mm/day) are considered light, the intermediate bin (5-10 mm/day) moderate and the last two bins (10-20 and 20+ mm/day) intense precipitation events. The top row shows the climatological average of the distribution in terms of percent frequency of occurrence, the second row shows the accumulated precipitation emanating from each intensity bin during the period of calculation, while the lower rows show the anomalies in the frequency of occurrence of each intensity class, averaged over the strong El Niño (*NINOA*) and La Niña (*NINOA*) years respectively. As in the onset calculations, the years used for the ENSO anomalies are the years

(0) for CAM and CAR, and years (+) for NAMZ and MEX, these being the years when ENSO forcing is maximum in the respective regions.

In the CAR region (Figure 2.3a,e,i,m) the climatological intensity distribution of precipitation during the rainy season is well simulated by RCA, except for a small underestimate in the 5-10 mm/day category and a small over-estimate in the 20+ mm/day category, the latter of which is responsible for the small positive bias in the annual cycle. ECMWF shows large under-estimates in the low intensity categories and over-estimate in the high intensity categories, consistent with the large wet bias seen in Figure 2.1a. Anomalies during ENSO years over CAR do show a small shift ( $\approx 1\%$  in each category), with more light precipitation events and less moderate and intense precipitation events. The converse is true for La Niña events, but the anomalies are of greater magnitude ( $\approx 1-2\%$  change in each category). The model reproduces most of the observed variability, with some deviations in the intense categories. The biases in the tail ends of the distribution in El Niño events explain the dry bias seen in May-July (0) *NINO4* of the annual cycle (see Figure 2.1e).

Over the CAM region (Figure 2.3b,f,j,n) the simulated distribution is not as accurate as in the CAR region, although the modal intensity (5-10 mm/day) is the same as in the observations and biases are less than 5% in each category. The anomalies related to ENSO are similar to those in the CAR region, but of larger magnitude. RCA again captures the overall shift in the distribution, as over CAR, but there is an excessive reduction in the frequency of very intense (20+ mm/day) precipitation pentads. In most categories the model is more accurate than ECMWF (relative to GPCP).

The NAMZ region (Figure 2.3c,g,k,o) has a more bimodal distribution, with most occurrences ( $\approx 75\%$ ) in the 5-20 mm/day range. RCA shows good agreement with observations, except in the two categories 5-10 and 10-20 mm/day, with an underestimate in the former balanced by an overestimate (in frequency) in the latter, explaining the wet bias in the second half of the rainy season. In ECMWF, although the pentad-mean precipitation is reasonable in the rainy season, the 5-10 and 10-20 mm/day categories

are not well represented. As in the two previous regions, the ENSO-related anomalies are clear and relatively well simulated.

To show the effect of using an interannually varying rainy season duration for the period of analysis, compared to using a fixed climatological rainy season, we plot the precipitation intensity distribution for the NAMZ region for a fixed rainy season, February-June, in Figure 2.4a,c,e,g. The climatological distribution is generally similar, but shows a shift towards lighter precipitation events, due to the increased inclusion of dry days in the distribution during years when the rainy season is delayed. The ENSO related shifts in the distribution are larger (by a factor of almost two) compared to the previously discussed results. RCA simulates most of the anomalies, but again shows some discrepancies mainly in the 5-10 and 20+ mm/day categories. As the variability is greater using this method, we conclude that the variability in the intensity distribution in the rainy season over NAMZ is due to both changes in the timing (onset and demise) of the rainy season, as well as changes in the distribution within the (interannually variable) rainy season. Over the CAR and CAM regions the two methods show similar anomalies (not shown), therefore in these regions we conclude that changes in the intensity distribution are mostly due to changes *within* the rainy season and not changes in the timing.

The final region, MEX (Figure 2.3d,h,l,p), having a much drier climate, has an observed and modeled modal intensity in the no-rain (0-1 mm/day) category. The model shows a small bias towards more dry, less moderate and more extreme events. With regard to changes in the intensity distribution associated with ENSO, our results show no clear signal, which should be expected recalling that the main documented ENSO impact occurs in October (0)-March (+), outside of the rainy season in MEX. In this region ECMWF results are comparable to observations.

As the ENSO-related variability in the MEX region is primarily in the dry season, we show in Figure 2.4b,d,f,h the intensity distribution during January-March and the anomalies in the same months for years (+) of the ENSO events. The modal intensity

is still in the dry (0-1 mm/day) category, but with a much larger intensity of  $\approx 70\%$ . All categories are well simulated by RCA. The anomalies in the El Niño years are now apparent (although marginally in RCA), with a shift towards fewer no-rain events and more events in the 2.5-20 mm/day range, accounting for a wetter dry season. In the La Niña years the shift is more dramatic and better captured by the model. As there are more consistent anomalies associated with ENSO (Compared to Figure 2.3), we conclude that ENSO has an impact on the intensity distribution of precipitation during the dry season only.

The limited temporal extent of high-resolution pentad (and daily) datasets such as TRMM is the main reason that GPCP was used as the primary observational dataset in this study. This limits the assessment of the benefits accruing from the increased resolution of a RCM. Here we briefly present results for the 1998-2004 period, comparing the  $0.33^\circ$  version of RCA to a lower-resolution version of the model run at  $1.0^\circ$  (RCA1) as well as high-resolution TRMM and low-resolution GPCP as reference (all interpolated to a  $1^\circ$  grid). Figure 2.5 shows the climatological frequency of occurrence and accumulated precipitation for each intensity bin for regions CAR and NAMZ only, during their respective rainy season. In most cases, RCA is closer to both TRMM and GPCP than the lower-resolution simulation RCA1. For example, RCA1 is the clear outlier in the 5-10 and 20+ mm/day categories for both regions. RCA1 shows excessive frequency and accumulation in the 20+ mm/day category, similar to ECMWF (Figure 2.3a,b,e,f). It is worth noting here that the model used in generating the ERA-40/ECMWF analysis data set used in this study has a resolution comparable to RCA1. The high-resolution TRMM and lower-resolution GPCP are in general accordance when spatially averaged. This is even more evident when looking at the accumulation plots, with differences of less than 100mm in each category. These points lead to the following conclusions : 1) RCA is more realistic at  $0.33^\circ$  than  $1.0^\circ$  in simulating the precipitation intensity distribution ; 2) GPCP pentad data at  $2.5^\circ$  resolution are reliable enough to be used as an observational surrogate for comparison with high-resolution data, when spatially averaged over relatively small regions and 3) RCA1 and ECMWF both have a tendency to

overestimate the frequency of intense precipitation in regions CAR and NAMZ.

### 2.3.3.2 Spatial Maps of Precipitation Intensity

As a final evaluation of RCA's ability to simulate the intensity distribution of precipitation and its changes due to ENSO forcing, we plot spatial maps showing the occurrences of pentad-mean precipitation intensity greater than 10 mm/day (intense precipitation events), along with changes in the occurrence of these events, expressed as deviations in percent from the climatological occurrence, for El Niño and La Niña years separately. Figure 2.6 emphasizes the rainy season in the northern portion of the domain, with the top row showing climatological results during the fixed July-September months and the two bottom rows showing the *NINOA* and *NINAA* of above 10 mm/day occurrences for the months July-September (0), when anomalies are important in Central America and the Caribbean. The columns show in order GPCP, ECMWF and RCA. We also show in Figure 2.7 the climatological values for the shorter 1998-2004 period for RCA, RCA1, GPCP and TRMM as an additional high-resolution comparison.

In the climatological mean for the 1979-2004 period (Figure 2.6a,b,c) we clearly see the location of the ITCZ, around 10°N, with over 40% of the total rainfall coming from pentad-mean rainfall rates greater than 10 mm/day. RCA has a slight eastward shift in the east Pacific and an enhanced ITCZ in the Atlantic, similar to the seasonal averages compared to the monthly GPCP dataset (see TJ2008a). The east Pacific ITCZ is severely over-estimated in ECMWF, and somewhat in the west Atlantic. Both RCA and ECMWF show the same overestimate of intense precipitation occurrence (compared to GPCP) in the tropical west Atlantic. This is close to the lateral boundary in RCA where the model is relaxed towards the ECMWF driving atmospheric fields. The commonality of RCA and ECMWF precipitation in this region may therefore be a result of errors in the atmospheric and dynamical forcing in the ECMWF analyses. RCA also shows more occurrences ( $\approx 5-10\%$ ) of intense precipitation events in the Caribbean and Gulf of Mexico when compared to GPCP, consistent with the wet bias in the seasonal cycle. The

higher occurrence of intense precipitation in this region is however more consistent with the TRMM dataset for the period 1998-2004 (see Figure 2.7). The lower-resolution model RCA1 also exhibits an excessive east Pacific ITCZ in the 1998-2004 period, similar to ECMWF (Figures 2.6b and 2.7d). There is also a clear positive bias in orographically forced rainfall in RCA1 (clearly seen in northern South America, Figure 2.7d), predominantly related to high intensity precipitation classes (as seen in Figure 2.5). We believe this is linked to problems with an accurate representation of resolved scale vertical velocity over mountainous regions and its role in the Kain-Fritsch convective trigger function (further explanation is given in section 5 of TJ2008a). Over northern South America RCA shows a small positive frequency bias ( $\approx 10-20\%$ ) compared to both GPCP and TRMM, which is consistent with the wet bias in the annual cycle and positive bias in the 10+ mm/day intensity categories over the NAMZ region.

Looking at the *NINO4* of the intense precipitation events (Figure 2.6d,e,f), the spatial structure and magnitude of the anomalies are generally well simulated. The southern half of the east Pacific ITCZ shows a positive anomaly of 20% (i.e. 20% more occurrences of precipitation  $> 10$  mm/day). Most regions north of this exhibit a negative anomaly of 10% on average (attributable to changes in the Hadley circulation). Both the RCA and ECMWF anomalies in this region are generally of the correct sign, but larger than the GPCP values. There are small negative anomalies in northern South America. Anomalies are slightly exaggerated in RCA and ECMWF over the Caribbean, Central America and northern Mexico.

The *NINA4* plots (Figure 2.6g,h,i) show almost inverse anomalies. In the tropical east Pacific and Atlantic oceans negative anomalies are greater and more widespread in RCA than in GPCP. The weakened descending branch of the Hadley circulation (mostly over Mexico and the Caribbean) leads to positive rainfall anomalies of +10-20% during La Niña years. Positive anomalies are slightly over-estimated over the Caribbean in RCA, while there is a severe over-estimate in ECMWF (also seen in the histograms for the CAR region in Figure 2.3m). Northeast South America, and parts of the NAMZ domain,

see a positive anomaly of  $\approx 10\%$  corresponding to changes in the Walker circulation during La Niña events, while regions south of that show a negative anomaly of  $\approx 5\%$ , which while captured is more widespread in RCA. RCA shows a distinctive rainshadow effect on the eastern slope of the Andes, which is marginally seen in the observations.

## 2.4 Discussion and Conclusions

We have evaluated the performance of the Rossby Center Regional Atmospheric Model in simulating subseasonal statistics of pentad-mean precipitation, in particular the interannual variability of pentad-mean rainfall associated with ENSO forcing. The annual cycle is well simulated by the model, except for a wet bias starting in the middle of the observed rainy season over the northern Amazon. Anomalies associated with ENSO are also generally well simulated in the four regions analysed, at least during the periods of well-known ENSO forcing. There are a few exceptions to this, notably before the onset of the rainy season in Central America and the Caribbean, where RCA shows excessive dry conditions in El Niño years and the converse in La Niña years.

The timing of the rainy season (onset, demise and duration) is found to be well simulated by the model, with biases of usually less than two weeks. One problem is found in the northern Amazon where the model shows a later onset and demise of the rainy season, due to a general wet bias and double maxima in the annual cycle of precipitation. Over the MEX region the demise of the rainy season is three weeks early in RCA compared to observations. One of the main changes induced by ENSO is an early/late demise in the rainy season over Central America and the Caribbean for El Niño/La Niña year (0) respectively. Northern Amazon experiences a late/early onset of the rainy season for El Niño/La Niña years (+) respectively and to a lesser extent an early/late demise. In these latter three regions (CAR, CAM and NAMZ) the duration of the rainy season is shorter/longer in the relevant El Niño/La Niña years, due to changes in the onset and demise dates. Over the MEX region there is an early demise in the years (+) of La Niña events and an early/late onset during El Niño/La Niña years respectively, consistent

with wet/dry anomalies during the dry season. These changes in the timing result in a longer/shorter rainy season in El Niño/La Niña years (+). All of these modulations in the timing of the rainy season associated with ENSO forcing are generally well captured by RCA.

The climatological, pentad-mean intensity distribution of precipitation during the rainy season is generally well simulated by the model, although a model wet bias over northern Amazon is associated with an over-estimate in the frequency of intense precipitation events (10+ mm/day). Overall, RCA adequately simulates the documented anomalies in rainfall intensity associated with ENSO forcing. The periods when the model disagrees with observations generally lie outside of these strongly forced periods, when predictability is limited. Seasonal mean dry anomalies are associated with a shift in the pentad-mean intensity distribution, with an increased frequency of light intensity events and a decreased frequency of intense events, the converse is true for wet seasonal anomalies. Over the northern Amazon ENSO induces both changes in the *timing* of the rainy season as well as changes in the intensity distribution *within* the shorter/longer rainy season. Over Central America and the Caribbean changes are mainly in the distribution *within* the rainy season, while changes in the rainy season length are less important. Finally, changes in the intensity distribution over MEX are only seen in the dry season, this being the period when ENSO anomalies have a impact over this region.

In the two parts of this study we have evaluated the ability of RCA to downscale SST and large-scale atmospheric anomalies over the tropical Americas associated with ENSO variability, when RCA is forced by observed SST and analysed LBCs. This has been done both for seasonal mean precipitation and subseasonal (pentad) rainfall. We have found that RCA offers a downscaling improvement over the driving LBC data (ECMWF) in terms of precipitation, and that the high resolution of  $0.33^\circ$  offers more realistic results than a lower-resolution version (at  $1.0^\circ$ ). These first results are encouraging in the context of downscaling accurate large-scale circulation anomalies. Further work in this area will involve running RCA with lateral boundary forcing obtained from a suite

of GCM hindcasts to assess the combined ability of a GCM-RCM couplet to simulate regional-scale interannual variability of precipitation over the tropical Americas.

*Acknowledgments.*

We wish to thank the Servicio Meteorológico Nacional de México for generously providing station precipitation observations for Mexico. U.S. precipitation data are from the U.S. Cooperative Observing Network, and were obtained from the National Climatic Data Center. We also thank Dave Allured and Brant Liebmann for preparing and providing the gridded dataset for daily precipitation over North America and Sara A. Rauscher for her insight and suggestions. We also acknowledge the assistance of Anders Ullerstig and Patrick Samuelsson of the Rossby Center at the Swedish Meteorological and Hydrological Institute (SMHI) in preparing the lateral and surface boundary conditions used to force RCA. RCA integrations were performed at the National Supercomputer Centre in Linköping, Sweden. This research was funded by CLIVAR grant 201649, NSERC grant RGPIN/327250-2006, CFCAS grant NW CRCMD and Ouranos Inc. ECMWF ERA-40 data used in this study have been provided by ECMWF.

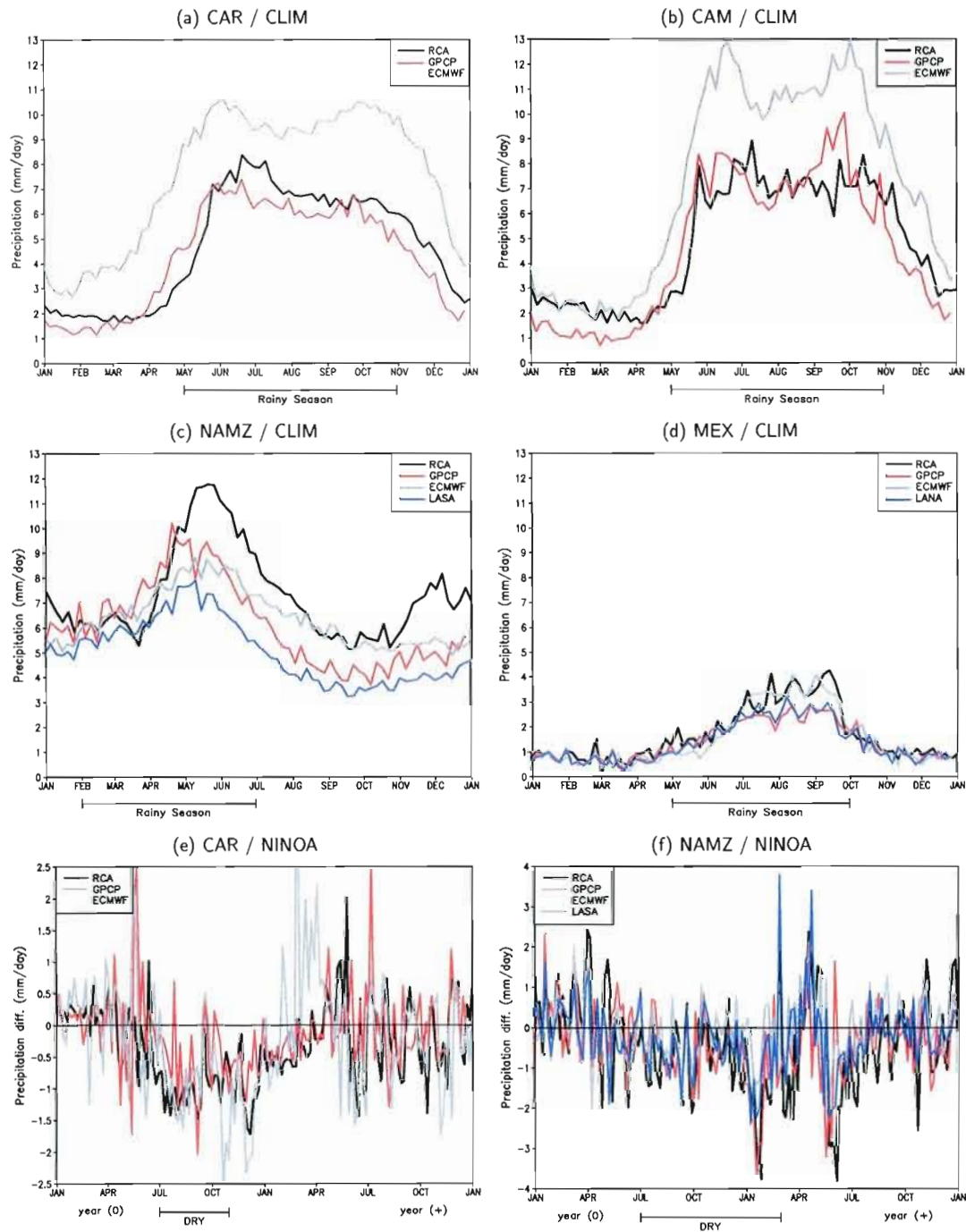


**Figure 2.1** Spatial mean climatological precipitation (top rows) and El Niño anomalies of precipitation (bottom row), annual cycle by region over land (mm/day). The duration of the climatological rainy season and the typical period and impact (wet/dry) of ENSO variability are indicated for each region on the x-axis.

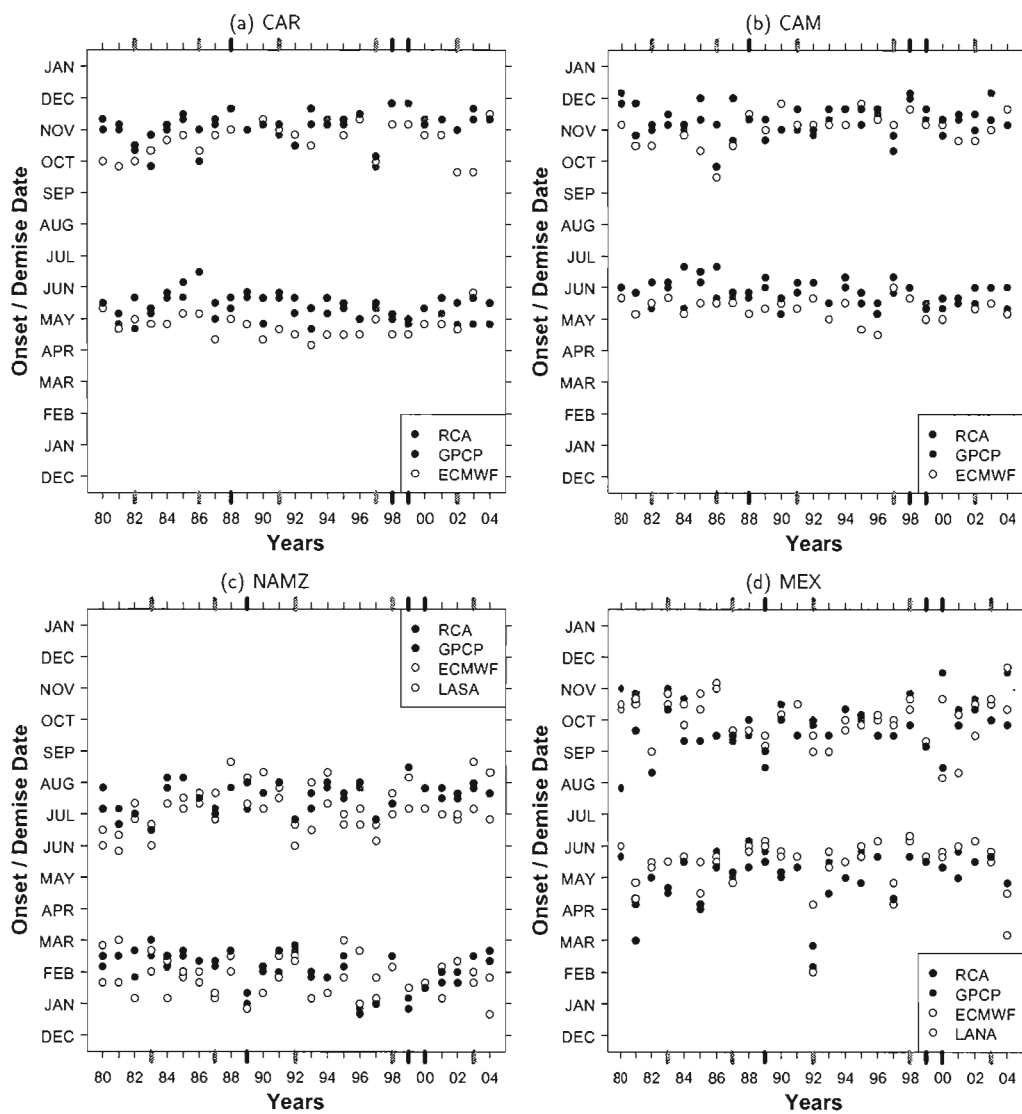
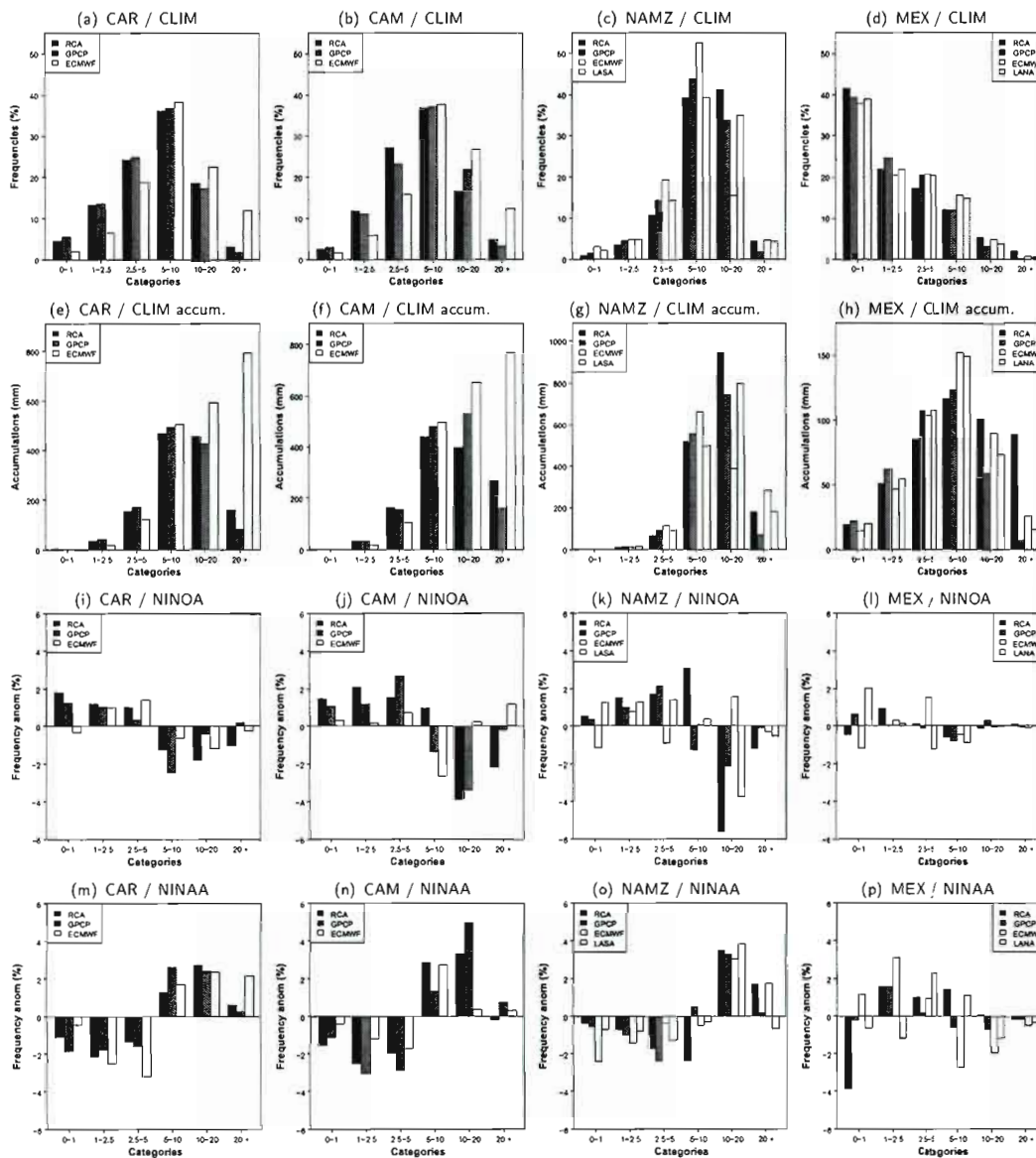
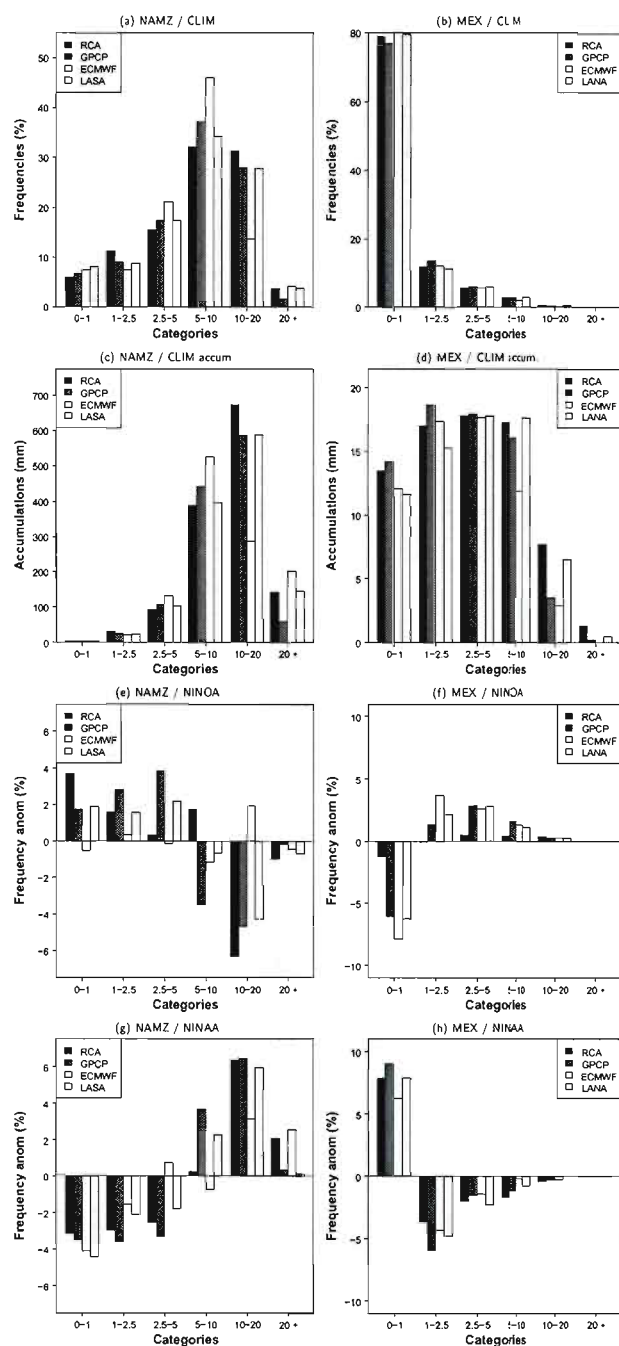


Figure 2.2 Onset and demise dates of the rainy season over land by region. Where a mark is not visible it is coincident with another mark. El Niño years are shown in large grey tick marks and La Niña years in large black tick marks on the x-axis.



**Figure 2.3** Precipitation intensity distribution (% of pentads) over land during yearly computed rainy seasons / climatological frequency of occurrence (top row), climatological accumulated precipitation for each intensity bin (second row) and anomalies in binned frequency of occurrence for El Niño and La Niña years (bottom rows) / regions CAR, CAM, NAMZ and MEX (columns). The scales on the y-axis are different in each plot.



**Figure 2.4** As Figure 2.3 but for NAMZ region using a fixed rainy season February-July (left column), MEX region using a fixed dry season January-March (right column).

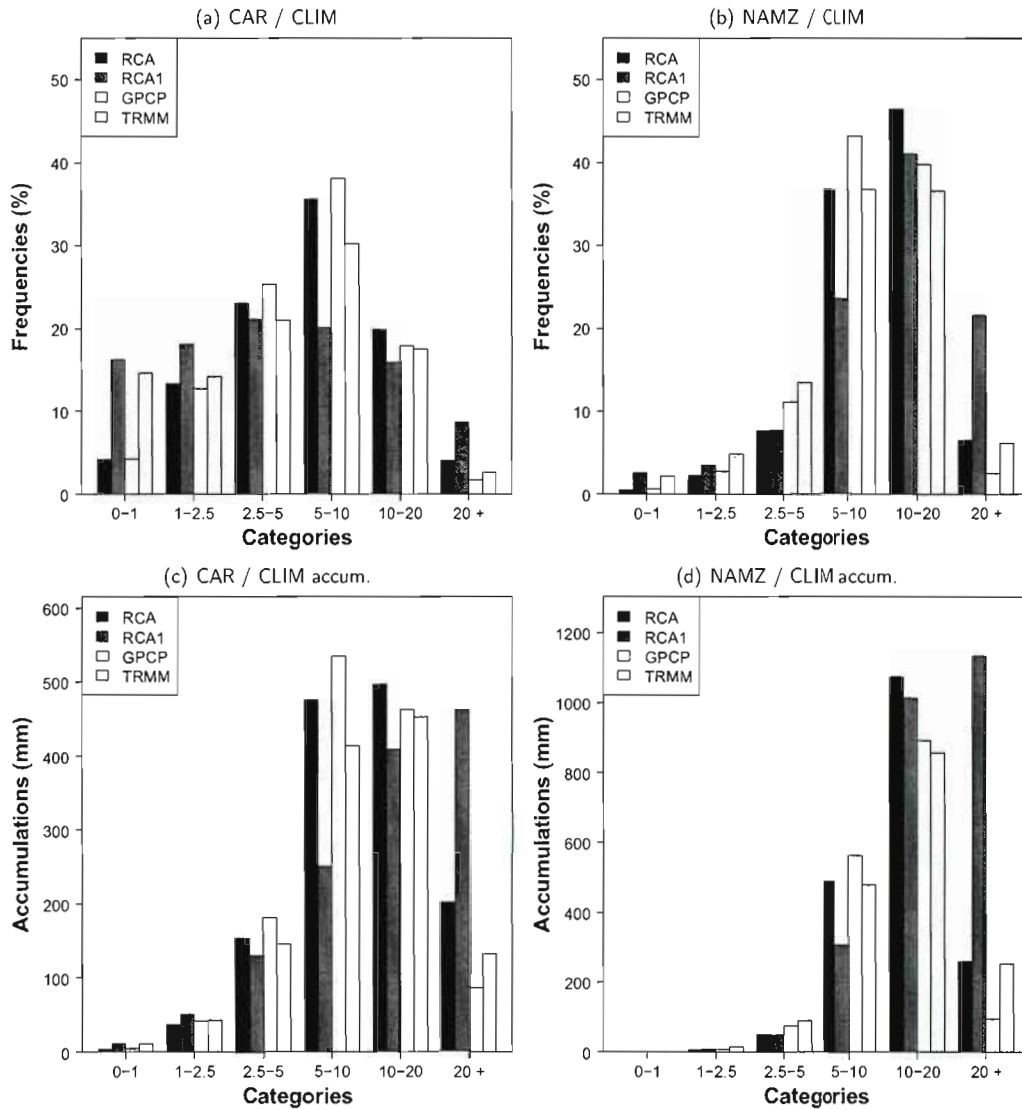


**Figure 2.5** Precipitation intensity distribution (% of pentads) over land during yearly computed rainy seasons during the 1998-2004 period / climatological frequency of occurrence (top row), climatological accumulated precipitation for each intensity bin (bottom row) / regions CAR and NAMZ (left and right columns). The scales on the y-axis are different in each plot.

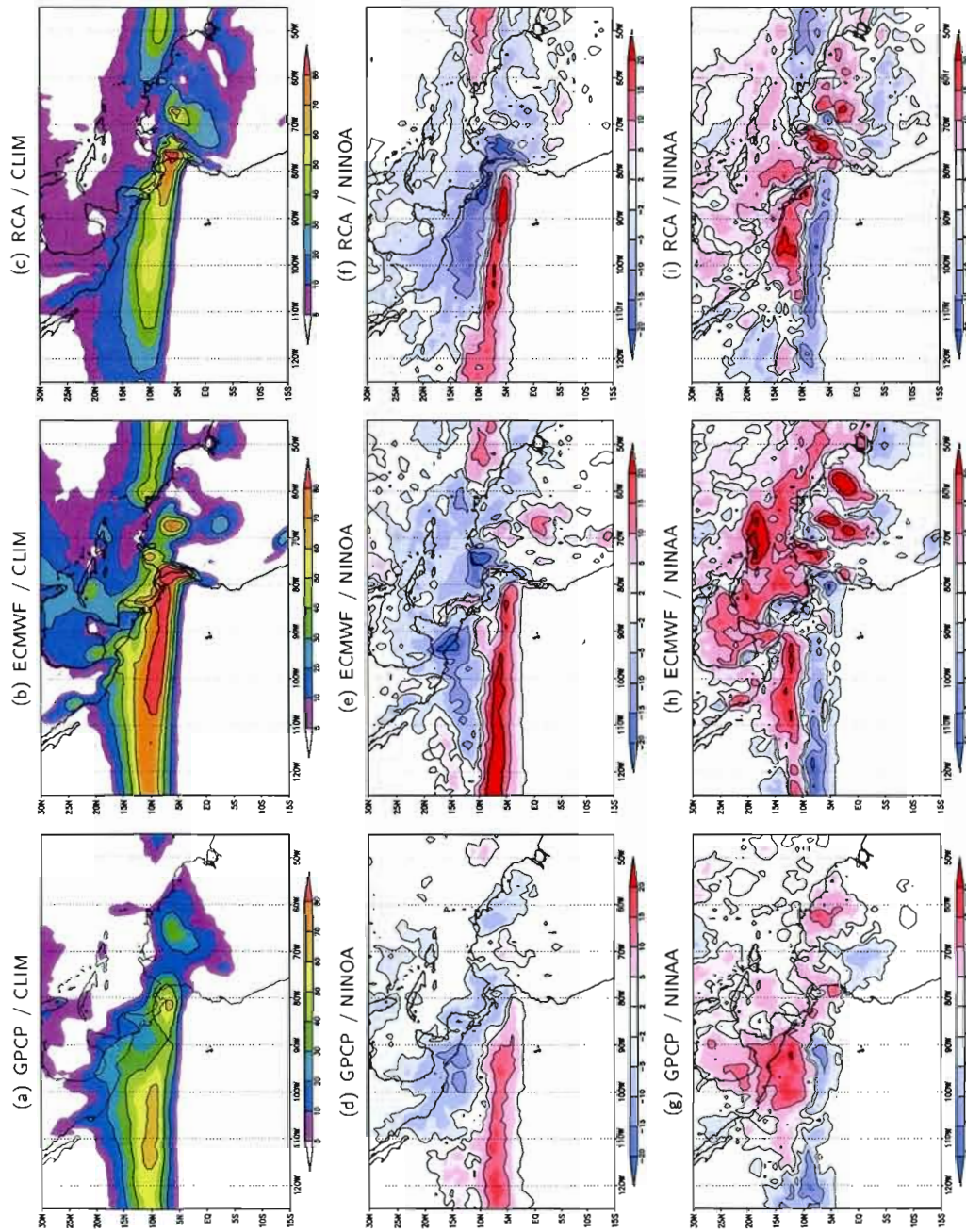


**Figure 2.6** Frequency of occurrence of pentad-mean precipitation in excess of 10 mm/day (in % of total precipitation intensity occurrence) for June-September / GPCP, ECMWF and RCA (columns) / Climatology (top row), El Niño anomalies (*NINOA*) during JAS(0) season (middle row) and La Niña anomalies (*NINAA*) during JAS(0) season (bottom row).

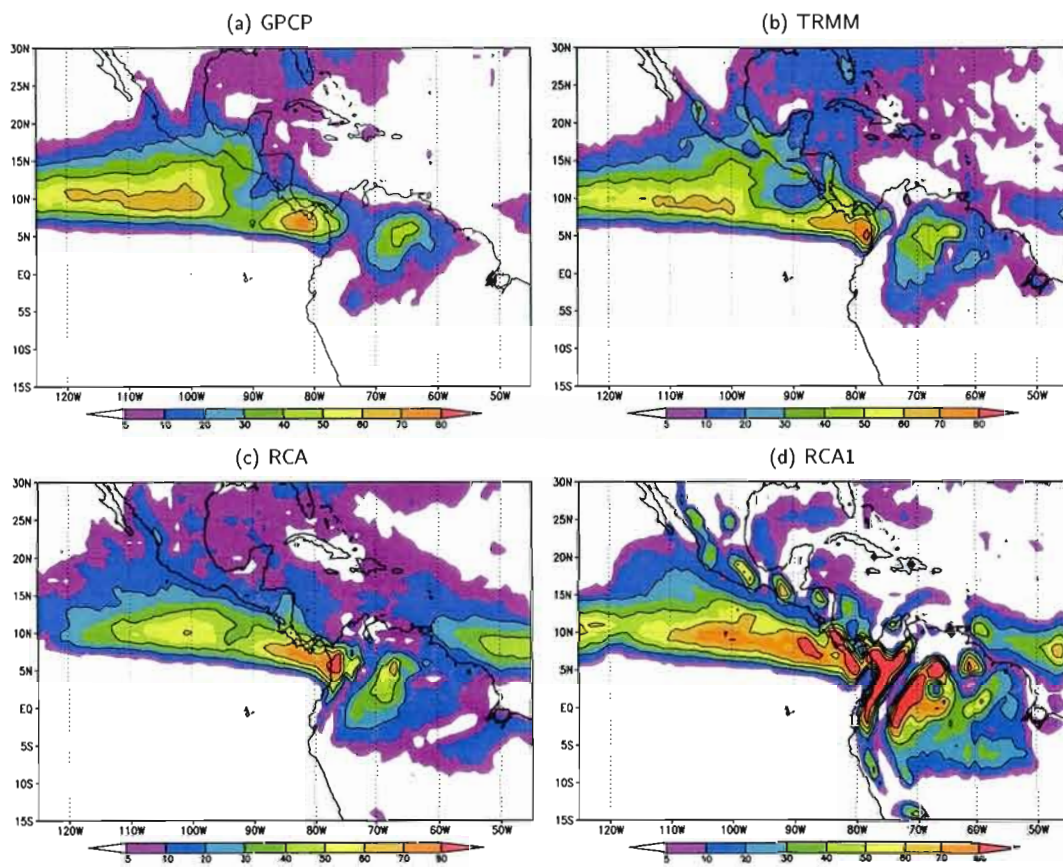


**Figure 2.7** Frequency of occurrence of pentad-mean precipitation in excess of 10 mm/day (in % of total precipitation intensity occurrence) for June-September during the 1998-2004 period.

**Table 2.1** Climatological Onset and Demise (month-day) and Length (in days) of Rainy Season by Region and changes (in days) in the Onset, Demise and Length for El Niño and La Niña years.

Region	Data	Climatology			El Niño changes			La Niña changes		
		Onset	Demise	Length	Onset	Demise	Length	Onset	Demise	Length
<b>CAR</b>	GPCP	05-06	11-02	180	0	-15	-15	-5	+10	+15
	ECMWF	04-26	10-18	175	0	-15	-15	-5	+15	+20
	RCA	05-16	11-02	170	+10	-20	-30	-5	+20	+25
<b>CAM</b>	GPCP	05-21	11-07	170	0	-5	-5	0	+10	+10
	ECMWF	05-11	10-28	170	+5	-10	-15	0	+15	+15
	RCA	05-31	11-07	160	+10	-15	-25	-10	+10	+20
<b>NAMZ</b>	GPCP	01-31	07-10	160	+10	-15	-25	-25	+10	+35
	ECMWF	02-05	07-15	160	0	0	0	-20	+10	+30
	LASA	01-16	06-30	165	+10	-10	-20	-15	+5	+20
	RCA	02-05	07-20	165	+15	-15	-30	-30	+15	+45
<b>MEX</b>	GPCP	05-11	10-03	145	-15	+5	+20	+10	-15	-25
	ECMWF	05-16	09-23	130	-10	+5	+15	+10	-30	-40
	LANA	05-11	10-03	145	-15	+5	+20	+10	-10	-20
	RCA	05-01	09-13	135	-5	+10	+15	+15	-20	-35

## CONCLUSION

Cette étude de sensibilité du modèle régional du climat RCA a démontré que ce modèle reproduit la majorité des caractéristiques climatiques de la précipitation dans les tropiques américaines à l'échelle saisonnière et intrasaisonnière. Nous avons étudié la performance du modèle à simuler les moyennes climatiques ainsi que les anomalies attribuables au phénomène ENSO. De façon générale la simulation du modèle est plus réaliste en terme de précipitation que celle fournie par les données de pilotage (les réanalyses ERA-40 de ECMWF). RCA reproduit relativement bien le cycle annuel de la précipitation à l'échelle saisonnière, ainsi que les statistiques intrasaisonnières telles que la distribution de la précipitation en terme d'intensité et les dates de début et fin de la saison des pluies. Quelques problèmes ont néanmoins été identifiés, soit une mauvaise distribution spatiale de la sécheresse relative au « Mid-Summer Drought » (MSD) en Amérique Centrale et un excès de précipitation à partir du milieu de la saison des pluies dans le Nord de l'Amazonie, ce qui a un effet sur la simulation de la fréquence des journées d'intensité modérée et forte, ainsi que sur les dates de la saison des pluies.

Pour ce qui est de la simulation des anomalies attribuables à ENSO, les anomalies saisonnières de précipitation identifiées dans la littérature scientifique sont majoritairement bien simulées par le modèle RCA. Le modèle simule bien les changements liés à la distribution de l'intensité des précipitations ainsi que les transitions entre la saison des pluies et la saison sèche dans les différentes régions-clé du domaine. Règle générale, une sécheresse durant la saison des pluies sera accompagnée d'une réduction des journées d'intensité modérée à forte et à un raccourcissement de la durée de la saison des pluies, et vice-versa. Le modèle simule des anomalies saisonnières légèrement excessives autour de l'Amérique Centrale avant le déclenchement observé de la saison des pluies, ce qui amène une erreur sur la simulation de la date de début de la saison des pluies.

Le modèle régional du climat Suédois RCA a été développé et testé dans des régions nordiques. Cette première validation de RCA dans les tropiques américaines démontre que ce modèle, lorsque piloté par les réanalyses ERA-40 de ECMWF et SST observées, permet de bien simuler la précipitation et sa variabilité due à ENSO dans les tropiques américaines à l'échelle saisonnière et intrasaisonnière. Une suite logique à ce projet serait d'utiliser RCA avec la même configuration, mais en utilisant comme conditions aux frontières les champs atmosphériques et SST provenant d'un MCG. Une autre voie à explorer serait l'emploi d'une technique d'ensemble qui permettrait de réduire la variabilité interne du modèle et donnerait des indications sur la robustesse des simulations. Ces deux méthodes font partie intégrante d'une véritable prévision saisonnière dont les bienfaits sont importants pour les populations des régions tropicales, vulnérables aux aléas du climat. Rappelons ici que les anomalies saisonnières et intrasaisonnières importantes associées au phénomène ENSO ont un grand potentiel de prévisibilité dans les régions tropicales.

Une autre avenue intéressante serait de modifier ou agrandir le domaine de la simulation pour inclure le Nord-Est du Brésil, qui a été écarté de ce projet. En effet, la région aride du Nord-Est du Brésil est la région la plus sensible au forçage ENSO sur le continent américain, en plus d'être constitué d'une population fortement vulnérable et pauvre. De plus, comme les efforts du Brésil sont fortement concertés sur cette région, il existe plusieurs bases de données à relativement forte densité d'observations journalières telle que la base de Liebmann et Allured (LASA) utilisée sur l'Amérique du Sud dans le second article. Ceci permettrait d'effectuer une étude semblable sur les statistiques journalières et non à la fréquence du pentad comme il a été fait dans l'étude présentée ici.

## RÉFÉRENCES

- Aceituno, P. 1988. « On the Functioning of the Southern Oscillation in the South American Sector. Part I : Surface Climate », *Mon. Wea. Rev.*, vol. 116, no. 3, p. 505–524.
- Adams, D. K. et A. C. Comrie. 1997. « The North American Monsoon », *Bull. Amer. Meteor. Soc.*, vol. 78, no. 10, p. 2197–2213.
- Adler, R. F., G. J. Huffman, A. Chang, R. Ferraro, P.-P. Xie, J. Janowiak, B. Rudolf, U. Schneider, S. Curtis, D. Bolvin, A. Gruber, J. Susskind, P. Arkin, et E. Nelkin. 2003. « The Version-2 Global Precipitation Climatology Project (GPCP) Monthly Precipitation Analysis (1979-Present) », *J. Hydrometeor.*, vol. 4, no. 6, p. 1147–1167.
- Albrecht, B. A. 1981. « Parameterization of Trade-Cumulus Cloud Amounts », *J. Atmos. Sci.*, vol. 38, no. 1, p. 97–105.
- Alexander, M. A., I. Blade, M. Newman, J. R. Lanzante, N.-C. Lau, et J. Scott. 2002. « The Atmospheric Bridge : The Influence of ENSO Teleconnections on Air-Sea Interaction over the Global Oceans », *J. Climate*, vol. 15, no. 16, p. 2205–2231.
- Alfaro, E. J. 2002. « Some Characteristics of the Annual Precipitation Cycle in Central America and their Relationships with its Surrounding Tropical Oceans », *Top. Meteor. Oceanog.*, vol. 9, no. 2, p. 88–103.
- Barnston, A. G. et R. E. Livezey. 1987. « Classification, Seasonality and Persistence of Low-Frequency Atmospheric Circulation Patterns », *Mon. Wea. Rev.*, vol. 115, no. 6, p. 1083–1126.
- Chiang, J. C. H., Y. Kushnir, et S. E. Zebiak. 2000. « Interdecadal changes in eastern Pacific ITCZ variability and its influence on the Atlantic ITCZ », *Geophys. Res. Lett.*, vol. 27, no. 22, p. 3687–3690.
- Chou, S. C., J. F. Bustamante, et J. L. Gomes. 2005. « Evaluation of Eta Model seasonal precipitation forecasts over South America », *Nonlin. Processes Geophys.*, vol. 12, no. 4, p. 537–555.
- Cuxart, J., P. Bougeault, et J.-L. Redelsperger. 2000. « A turbulence scheme allowing for mesoscale and large-eddy simulations », *Quart. J. Roy. Meteor. Soc.*, vol. 126, no. 562, p. 1–30.
- Davies, H. C. 1976. « A lateral boundary formulation for multi-level prediction models », *Quart. J. Roy. Meteor. Soc.*, vol. 102, no. 432, p. 405–418.

- Deng, A., N. L. Seaman, et J. S. Kain. 2003. « A Shallow-Convection Parameterization for Mesoscale Models. Part I : Submodel Description and Preliminary Applications », *J. Atmos. Sci.*, vol. 60, no. 1, p. 34–56.
- Enfield, D. B. 1996. « Relationship of inter-American rainfall to tropical Atlantic and Pacific SST variability », *Geophys. Res. Lett.*, vol. 23, no. 23, p. 3305–3308.
- Enfield, D. B. et E. J. Alfaro. 1999. « The Dependence of Caribbean Rainfall on the Interaction of the Tropical Atlantic and Pacific Oceans », *J. Climate*, vol. 12, no. 7, p. 2093–2103.
- Enfield, D. B. et D. A. Mayer. 1997. « Tropical Atlantic sea surface temperature variability and its relation to El Niño-Southern Oscillation », *J. Geophys. Res.*, vol. 102, no. C1, p. 929–945.
- Fernandez, J. P. R., S. H. Franchito, et V. B. Rao. 2006a. « Simulation of the summer circulation over South America by two regional climate models. Part I : Mean climatology », *Theor. Appl. Climatol.*, vol. 86, no. 1, p. 247–260.
- . 2006b. « Simulation of the summer circulation over South America by two regional climate models. Part II : A comparison between 1997/1998 El Niño and 1998/1999 La Niña events », *Theor. Appl. Climatol.*, vol. 86, no. 1, p. 261–270.
- Fu, R., R. E. Dickinson, M. Chen, et H. Wang. 2001. « How Do Tropical Sea Surface Temperatures Influence the Seasonal Distribution of Precipitation in the Equatorial Amazon ? », *J. Climate*, vol. 14, no. 20, p. 4003–4026.
- Giannini, A., M. A. Cane, et Y. Kushnir. 2001a. « Interdecadal Changes in the ENSO Teleconnection to the Caribbean Region and the North Atlantic Oscillation », *J. Climate*, vol. 14, no. 13, p. 2867–2879.
- Giannini, A., J. C. H. Chiang, M. A. Cane, Y. Kushnir, et R. Seager. 2001b. « The ENSO Teleconnection to the Tropical Atlantic Ocean : Contributions of the Remote and Local SSTs to Rainfall Variability in the Tropical Americas », *J. Climate*, vol. 14, no. 24, p. 4530–4544.
- Giannini, A., Y. Kushnir, et M. A. Cane. 2000. « Interannual Variability of Caribbean Rainfall, ENSO, and the Atlantic Ocean », *J. Climate*, vol. 13, no. 2, p. 297–311.
- Gochis, D. J., W. J. Shuttleworth, et Z.-L. Yang. 2002. « Sensitivity of the Modeled North American Monsoon Regional Climate to Convective Parameterization », *Mon. Wea. Rev.*, vol. 130, no. 5, p. 1282–1298.
- Goddard, L., S. J. Mason, S. E. Zebiak, C. Ropelewski, R. Basher, et M. A. Cane. 2001. « Current approaches to seasonal to interannual climate predictions », *Int. J. Climatol.*, vol. 21, no. 9, p. 1111–1152.
- Hernandez, J. L., J. Srikishen, D. J. Erickson, R. Oglesby, et D. Irwin. 2006. « A regional climate study of Central America using the MM5 modeling system : results and comparison to observations », *Int. J. Climatol.*, vol. 26, no. 15, p. 2161–2179.

- Higgins, R. W., Y. Chen, et A. V. Douglas. 1999. « Interannual Variability of the North American Warm Season Precipitation Regime », *J. Climate*, vol. 12, no. 3, p. 653–680.
- Horel, J. D. et J. M. Wallace. 1981. « Planetary-Scale Atmospheric Phenomena Associated with the Southern Oscillation », *Mon. Wea. Rev.*, vol. 109, no. 4, p. 813–829.
- Huffman, G. J., R. F. Adler, D. T. Bolvin, G. Gu, E. J. Nelkin, K. P. Bowman, Y. Hong, E. F. Stocker, et D. B. Wolff. 2007. « The TRMM Multisatellite Precipitation Analysis (TMPA) : Quasi-Global, Multiyear, Combined-Sensor Precipitation Estimates at Fine Scales », *J. Hydrometeor.*, vol. 8, no. 1, p. 38–55.
- Huffman, G. J., R. F. Adler, M. M. Morrissey, D. T. Bolvin, S. Curtis, R. Joyce, B. McGavock, et J. Susskind. 2001. « Global Precipitation at One-Degree Daily Resolution from Multisatellite Observations », *J. Hydrometeor.*, vol. 2, no. 1, p. 36–50.
- Jones, C. G., U. Willén, A. Ullerstig, et U. Hansson. 2004. « The Rossby Centre Regional Atmospheric Climate Model Part I : Model Climatology and Performance for the Present Climate over Europe », *Ambio*, vol. 33, no. 4, p. 199–210.
- Kain, J. S. 2004. « The Kain-Fritsch Convective Parameterization : An Update », *J. Appl. Meteor.*, vol. 43, no. 1, p. 170–181.
- Kain, J. S. et J. M. Fritsch. 1990. « A One-Dimensional Entraining/Detraining Plume Model and Its Application in Convective Parameterization », *J. Atmos. Sci.*, vol. 47, no. 23, p. 2784–2802.
- . 1993. *Convective parameterizations for Mesoscale Models : The Kain-Fritsch scheme*. Coll. « The representation of cumulus convection in numerical models, Meteor. Monogr. », no 46, p. 165–170. Amer. Meteor. Soc.
- Kjellström, E., L. Bärring, S. Gollvik, U. Hansson, C. Jones, P. Samuelsson, M. Rumukainen, A. Ullerstig, U. Willén, et K. Wyser. 2005. « A 140-year simulation of European climate with the new version of the Rossby Centre regional atmospheric climate model (RCA3) », *SMHI Reports Meteorology and Climatology*, no. 108. SMHI, SE-60176 Norrköping, Sweden, 54 pp.
- Kousky, V. E., M. T. Kagano, et I. Cavalcanti. 1984. « A review of the Southern Oscillation : oceanic-atmospheric circulation changes and related rainfall anomalies », *Tellus A*, vol. 36A, no. 5, p. 490–504.
- Latif, M., D. Anderson, T. Barnett, M. Cane, R. Kleeman, A. Leetmaa, J. O'Brien, A. Rosati, et E. Schneider. 1998. « A review of the predictability and prediction of ENSO », *J. Geophys. Res.*, vol. 103, no. C7, p. 14,375–14,393.
- Lenderink, G. et A. A. M. Holtslag. 2004. « An updated length-scale formulation for turbulent mixing in clear and cloudy boundary layers », *Quart. J. Roy. Meteor. Soc.*, vol. 130, no. 604, p. 3405–3427.
- Liebmann, B. et D. Allured. 2005. « Daily Precipitation Grids for South America », *Bull. Amer. Meteor. Soc.*, vol. 86, no. 11, p. 1567–1570.

- Liebmann, B. et J. A. Marengo. 2001. « Interannual Variability of the Rainy Season and Rainfall in the Brazilian Amazon Basin », *J. Climate*, vol. 14, no. 22, p. 4308–4318.
- Magaña, V., J. A. Amador, et S. Medina. 1999. « The Midsummer Drought over Mexico and Central America », *J. Climate*, vol. 12, no. 6, p. 1577–1588.
- Magaña, V. et E. Caetano. 2005. « Temporal evolution of summer convective activity over the Americas warm pools », *Geophys. Res. Lett.*, vol. 32, no. L02803.
- Magaña, V. O., J. L. Vázquez, J. L. Pérez, et J. B. Pérez. 2003. « Impact of El Niño on precipitation in Mexico », *Geofis. Int.*, vol. 42, no. 003, p. 313–330.
- Marengo, J., I. Cavalcanti, P. Satyamurty, I. Trosnikov, C. Nobre, J. Bonatti, H. Camargo, G. Sampaio, M. Sanches, A. Manzi, C. Castro, C. D’Almeida, L. Pezzi, et L. Candido. 2003. « Assessment of regional seasonal rainfall predictability using the CPTEC/COLA atmospheric GCM », *Climate Dyn.*, vol. 21, no. 5, p. 459–475.
- Marengo, J. A. 1992. « Interannual variability of surface climate in the Amazon basin », *Int. J. Climatol.*, vol. 12, no. 8, p. 853–863.
- Marengo, J. A. et S. Hastenrath. 1993. « Case Studies of Extreme Climatic Events in the Amazon Basin », *J. Climate*, vol. 6, no. 4, p. 617–627.
- Marengo, J. A., B. Liebmann, V. E. Kousky, N. P. Filizola, et I. C. Wainer. 2001. « Onset and End of the Rainy Season in the Brazilian Amazon Basin », *J. Climate*, vol. 14, no. 5, p. 833–852.
- Masson, V., J.-L. Champeaux, F. Chauvin, C. Meriguet, et R. Lacaze. 2003. « A Global Database of Land Surface Parameters at 1-km Resolution in Meteorological and Climate Models », *J. Climate*, vol. 16, no. 9, p. 1261–1282.
- Mitchell, T. D. et P. D. Jones. 2005. « An improved method of constructing a database of monthly climate observations and associated high-resolution grids », *Int. J. Climatol.*, vol. 25, no. 6, p. 693–712.
- Nobre, P. et J. Shukla. 1996. « Variations of Sea Surface Temperature, Wind Stress, and Rainfall over the Tropical Atlantic and South America », *J. Climate*, vol. 9, no. 10, p. 2464–2479.
- Onogi, K., J. Tsutsui, H. Koide, M. Sakamoto, S. Kobayashi, H. Hatsushika, T. Matsumoto, N. Yamazaki, H. Kamahori, K. Takahashi, S. Kadokura, K. Wada, K. Kato, R. Oyama, T. Ose, N. Mannoji, et R. Taira. 2007. « The JRA-25 Reanalysis », *J. Meteor. Soc. Japan*, vol. 85, p. 369–432.
- Palmer, T. N., A. Alessandri, U. Andersen, P. Cantelaube, M. Davey, P. Délecluse, M. Déqué, E. Díez, F. J. Doblas-Reyes, H. Feddersen, R. Graham, S. Gualdi, J.-F. Guérémy, R. Hagedorn, M. Hoshen, N. Keenlyside, M. Latif, A. Lazar, E. Maisonave, V. Marletto, A. P. Morse, B. Orfila, P. Rogel, J.-M. Terres, et M. C. Thomson. 2004. « Development of a European Multi-Model Ensemble System for Seasonal to Inter-Annual Prediction (DEMETER) », *Bull. Amer. Meteor. Soc.*, vol. 85, no. 6, p. 853–872.

- Pan, Z., E. Takle, W. Gutowski, et R. Turner. 1999. « Long Simulation of Regional Climate as a Sequence of Short Segments », *Mon. Wea. Rev.*, vol. 127, no. 3, p. 308–321.
- Philander, S. G. 1990. *El Niño, La Niña, and the Southern Oscillation*. T. 46, série *International Geophysics Series*. San Diego, CA : Academic Press.
- Qian, J.-H., A. Seth, et S. Zebiak. 2003. « Reinitialized versus Continuous Simulations for Regional Climate Downscaling », *Mon. Wea. Rev.*, vol. 131, no. 11, p. 2857–2874.
- Räsänen, P., M. Rummukainen, et J. Räisänen. 2000. Modification of the HIRLAM radiation scheme for use in the Rossby Centre regional Atmospheric Climate model. Report 49, Department of Meteorology, University of Helsinki, 71 pp.
- Rasch, P. J. et J. E. Kristansson. 1998. « A Comparison of the CCM3 Model Climate Using Diagnosed and Predicted Condensate Parameterizations », *J. Climate*, vol. 11, no. 7, p. 1587–1614.
- Rauscher, S. A., A. Seth, B. Liebmann, J.-H. Qian, et S. J. Camargo. 2007. « Regional Climate Model-Simulated Timing and Character of Seasonal Rains in South America », *Mon. Wea. Rev.*, vol. 135, no. 7, p. 2642–2657.
- Ropelewski, C. F. et M. A. Bell. 2008. « Shifts in the Statistics of Daily Rainfall in South America Conditional on ENSO Phase », *J. Climate*, vol. 21, no. 5, p. 849–865.
- Ropelewski, C. F. et M. S. Halpert. 1987. « Global and Regional Scale Precipitation Patterns Associated with the El Niño/Southern Oscillation », *Mon. Wea. Rev.*, vol. 115, no. 8, p. 1606–1626.
- . 1989. « Precipitation Patterns Associated with the High Index Phase of the Southern Oscillation », *J. Climate*, vol. 2, no. 3, p. 268–284.
- . 1996. « Quantifying Southern Oscillation-Precipitation Relationships », *J. Climate*, vol. 9, no. 5, p. 1043–1059.
- Samuelsson, P., S. Gollvik, et A. Ullerstig. 2006. The land-surface scheme of the Rossby Centre regional atmospheric climate model (RCA3). Report in Meteorology 122, SMHI. SE-601 76 Norrköping, Sweden.
- Sardeshmukh, P. D., G. P. Compo, et C. Penland. 2000. « Changes of Probability Associated with El Niño », *J. Climate*, vol. 13, no. 24, p. 4268–4286.
- Sardeshmukh, P. D. et B. J. Hoskins. 1988. « The Generation of Global Rotational Flow by Steady Idealized Tropical Divergence », *J. Atmos. Sci.*, vol. 45, no. 7, p. 1228–1251.
- Savijärvi, H. 1990. « Fast Radiation Parameterisation Schemes for Mesoscale and Short-Range Forecast Models », *J. Appl. Meteor.*, vol. 29, p. 437–447.
- Seth, A., S. A. Rauscher, S. J. Camargo, J.-H. Qian, et J. S. Pal. 2007. « RegCM3 regional climatologies for South America using reanalysis and ECHAM global model driving fields », *Climate Dyn.*, vol. 28, no. 5, p. 461–380.

- Seth, A., M. Rojas, B. Liebmann, et J.-H. Qian. 2004. « Daily rainfall analysis for South America from a regional climate model and station observations », *Geophys. Res. Lett.*, vol. 31, p. L07213.
- Shukla, J. 1998. « Predictability in the Midst of Chaos : A Scientific Basis for Climate Forecasting », *Science*, vol. 282, no. 5389, p. 728–731.
- Shukla, J., J. Anderson, D. Baumhefner, C. Brankovic, Y. Chang, E. Kalnay, L. Marx, T. Palmer, D. Paolino, J. Ploshay, S. Schubert, D. Straus, M. Suarez, et J. Tribbia. 2000. « Dynamical Seasonal Prediction », *Bull. Amer. Meteor. Soc.*, vol. 81, no. 11, p. 2593–2606.
- Simmons, A., J. Wallace, et G. Branstator. 1983. « Barotropic Wave Propagation and Instability, and Atmospheric Teleconnection Patterns », *J. Atmos. Sci.*, vol. 40, no. 6, p. 1363–1392.
- Small, R. J. O., S. P. de Szoeki, et S.-P. Xie. 2007. « The Central American Midsummer Drought : Regional Aspects and Large-Scale Forcing », *J. Climate*, vol. 20, no. 19, p. 4853–4873.
- Smith, T. M. et R. W. Reynolds. 2004. « Improved Extended Reconstruction of SST (1854-1997) », *J. Climate*, vol. 17, no. 12, p. 2466–2477.
- Sun, L., D. F. Moncunill, H. Li, A. D. Moura, F. D. A. D. S. Filho, et S. E. Zebiak. 2006. « An Operational Dynamical Downscaling Prediction System for Nordeste Brazil and the 2002-04 Real-Time Forecast Evaluation », *J. Climate*, vol. 19, no. 10, p. 1990–2007.
- Taylor, M. A. et E. J. Alfaro. 2005. *Climate of Central America and the Caribbean*. Oliver, J. E., éditeur, Coll. « *The Encyclopedia of World Climatology* », p. 193–189. Netherlands : Springer.
- Taylor, M. A., D. B. Enfield, et A. A. Chen. 2002. « Influence of the tropical Atlantic versus the tropical Pacific on Caribbean rainfall », *J. Geophys. Res.*, vol. 107, no. C9, p. 3127.
- Tourigny, E. et C. Jones. 2008a. « An Analysis of Regional Climate Model Performance Over the Tropical Americas. Part I : Simulating Seasonal Variability of Precipitation Associated with ENSO Forcing », *Tellus A*. Accepté avec révisions (TeA-08-04-0037.R1).
- . 2008b. « An Analysis of Regional Climate Model Performance Over the Tropical Americas. Part II : Simulating Subseasonal Variability of Precipitation Associated with ENSO Forcing », *Tellus A*. Accepté avec révisions (TeA-08-04-0038.R1).
- Uppala, S., P. Kallberg, A. Simmons, U. Andrae, V. da Costa Bechtold, M. Fiorino, J. Gibson, J. Haseler, A. Hernandez, G. Kelly, X. Li, K. Onogi, S. Saarinen, N. Sokka, R. Allan, E. Andersson, K. Arpe, M. Balmaseda, A. Beljaars, L. van den Berg, J. Bidlot, N. Bormann, S. Caires, F. Chevallier, A. Dethof, M. Dragosavac, M. Fisher, M. Fuentes, S. Hagemann, E. Holm, B. Hoskins, L. Isaksen, P. Janssen, R. Jenne, A. McNally, J.-F. Mahfouf, J.-J. Morcrette, N. Rayner, R. Saunders,

- P. Simon, A. Sterl, K. Trenberth, A. Untch, D. Vasiljevic, P. Viterbo, et J. Woolen. 2005. « The ERA-40 re-analysis », *Quart. J. Roy. Meteor. Soc.*, vol. 131, p. 2961–3012.
- Wang, H.-J., R.-H. Zhang, J. Cole, et F. Chavez. 1999. « El Niño and the related phenomenon Southern Oscillation (ENSO) : The largest signal in interannual climate variation », *Proc. Natl. Acad. Sci. USA*, vol. 96, no. 20, p. 11071–11072.
- Xie, P., J. E. Janowiak, P. A. Arkin, R. Adler, A. Gruber, R. Ferraro, G. J. Huffman, et S. Curtis. 2003. « GPCP Pentad Precipitation Analyses : An Experimental Dataset Based on Gauge Observations and Satellite Estimates », *J. Climate*, vol. 16, no. 13, p. 2197–2214.
- Xie, S.-P., T. Miyama, Y. Wang, H. Xu, S. P. de Szoeki, R. J. O. Small, K. J. Richards, T. Mochizuki, et T. Awaji. 2007. « A Regional Ocean-Atmosphere Model for Eastern Pacific Climate : Toward Reducing Tropical Biases », *J. Climate*, vol. 20, no. 8, p. 1504–1522.
- Xu, J., X. Gao, J. Shuttleworth, S. Sorooshian, et E. Small. 2004. « Model Climatology of the North American Monsoon Onset Period during 1980–2001 », *J. Climate*, vol. 17, no. 20, p. 3892–3906.
- Xu, K.-M. et S. K. Krueger. 1991. « Evaluation of Cloudiness Parameterizations Using a Cumulus Ensemble Model », *Mon. Wea. Rev.*, vol. 119, no. 2, p. 342–367.
- Xu, K.-M. et D. A. Randall. 1996. « A Semiempirical Cloudiness Parameterization for Use in Climate Models », *J. Atmos. Sci.*, vol. 53, no. 21, p. 3084–3102.